

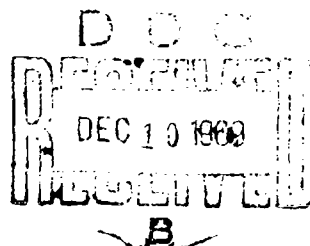
AD 697940

FORECAST METHODS FROM SATELLITE PHOTOGRAPHS

ISR-45



John C. Freeman
Principal Investigator
with
Pieter Feteris
Sam Rosenberg
Keith Veigas
Troxel Ballou



Institute for Storm Research, Inc./at the University of St. Thomas
3812 Montrose Boulevard
Houston, Texas 77006

Reproduced by the
CLEARINGHOUSE
for Federal Scientific & Technical
Information Springfield Va. 22151

June, 1969

This document has been prepared
for public release and sale
distribution is unlimited

FORECAST METHODS FROM SATELLITE PHOTOGRAPHS

Final Report

Submitted to Project FAMOS
Contract No. N 62306-68-C-0289
U.S. Fleet Weather Facility
Department of the Navy

ISR-45

John C. Freeman
Principal Investigator

Pieter Feteris

Sam Rosenberg

Keith Velgas and Troxel Ballou

Institute for Storm Research, Inc./at the University of St. Thomas
3812 Montrose Boulevard
Houston, Texas 77006
(713)-529-4891

June, 1969

ABSTRACT

Two models of atmospheric flow, "compensation" and "moist over-compensation" are found to be useful in the study of tropical weather in conventional and satellite observations. A numerical weather prediction model simulating important physical processes in the low latitudes is developed to test the feasibility of using ATS information to infer future weather distribution. Diagnostic studies using ATS films and conventional synoptic weather maps describe the weather situations in the Central North Pacific in terms of the theoretical models. Results of the prediction experiment and future use of ATS type data in numerical prediction models are discussed and application recommended. Appendix A gives a description of one method of following cloud motion in satellite photographs.

TABLE OF CONTENTS

ABSTRACT	ii
LIST OF ILLUSTRATIONS	iv
I. FORECAST METHODS FROM SATELLITE PHOTOGRAPHS	
A. Introduction	1
B. Compensation and Clouds	3
C. Moist Overcompensation	8
D. Moist Air Injection	12
E. Theory of Moisture Influx	14
F. Introduction of Moisture Into the Prediction Model	17
II. THE SYNOPTIC SITUATION FOR THE PREDICTION EXPERIMENT.	21
III. RESULTS OF THE NUMERICAL PREDICTION EXPERIMENTS	31
IV. ON THE FUTURE USE OF ATS TYPE DATA IN NUMERICAL PREDICTION MODELS	
A. Case Study	39
B. Use of Satellite Information in Numerical Weather Prediction	42
REFERENCES	47
APPENDIX A. A METHOD OF FOLLOWING PATTERN CLOUDS ON SEQUENTIAL SATELLITE PHOTOGRAPHS	49
APPENDIX B. SATELLITE OBSERVED CLOUDS AS STREAK LINES AND THE USE OF STREAK LINES AS A COORDINATE SYSTEM ..	59

LIST OF ILLUSTRATIONS

Figure		Page
1	Easterlies with no upper wind	4
2	Upper air trough causes inversion to rise	4
3	Upper air ridge causes inversion to lower	6
4	Upper air low cell modifies inversion	6
5	Prediction of inversion from satellite photographs	7
6	Schematic representation of undisturbed subtropical easterly flow underlying upper level westerlies	9
7	Compensation by upward adjustment	9
8	High level perturbation reflected at surface	9
9	Evolution of low level flow and cloud patterns subse- quent to Figure 8	9
10	Large scale moist overcompensation causes west winds at the surface	10
11	High level cloud streaming out of the tropics	13
12	Stages in a rising large scale cloud mass	15
13	Temperature distribution in dry air and in clouds	18
14	Surface chart 0000Z 7 April and ATS photo 2217Z 6 April 1967	22
15	500 mb streamline analysis chart 0000Z 7 April 1967	23
16	250 mb streamline analysis chart 0000Z 7 April 1967	24
17	Surface chart 0000Z 8 April and ATS photo 2340Z 7 April 1967	25
18	500 mb streamline analysis chart for 0000Z 8 April 1967	27

Figure		Page
19	250 mb streamline analysis chart for 0000Z 8 April 1967	28
20	ATS photo for 2223Z 8 April 1967.	29
21	ATS photo for 2251Z 9 April 1967.	30
22	Observed low level wind field u component 0000Z 7 April 1967.	32
23	Observed low level wind field v component 0000Z 7 April 1967.	33
24	Predicted low level wind field u component 0600Z 7 April 1967.	35
25	Predicted low level wind field v component 0600Z 7 April 1967.	36
26	Predicted height of easterlies 0600Z 7 April 1967	37
27	Surface chart 0000Z 28 March and ATS photo for 2252Z 29 March 1967	40
28	Surface chart 1800Z 28 March and ATS photo for 2137Z 28 March 1967	41
29	"Silent" conventional observation areas for cloud cover 0000Z 28 March 1967.	45
30	Binary digitized map of satellite radar cloud photograph	51
31	Section from Figure 30.	52
32	Example of procedure with actual data inserted	54
33	Figure 32, indicating secondary trend	55
34	Figure 32, indicating tertiary trends	56
35	ESSA digitized mosaic map from 2000Z 29 May 1969.	57
36	ESSA digitized mosaic map from 2000Z 30 May 1969.	57

I. FORECAST METHODS FROM SATELLITE PHOTOGRAPHS

John C. Freeman and Sam Rosenberg

A. Introduction

The objective of this study is to develop a numerical weather prediction model simulating important physical processes in the tropical and subtropical atmosphere which can be applied to data furnished by ATS satellite photographs, in order to test the feasibility of using ATS information to infer future weather distribution.

Parallel with the theoretical development of the prediction model, it was necessary to carry out preliminary diagnostic studies, using ATS films and microfilm copies of manuscript maps from 12 March to 31 May 1967. Only hemispheric NMC surface charts were available for the month of March, 1967. For the remainder of the period studied the maps prepared by the ESSA Weather Bureau in Honolulu were used. Analyses were made available for the surface, 700, 500 and 250 millibar levels.

The perusal of these data led to the selection of a sequence of weather (Section II) for the application of the numerical model described in Section I. The April case selected for the series of prediction experiments in Section III was one which is frequently observed over the tropical and subtropical oceans, with a typical broad zone of tropical easterlies. The series of ATS photos showed an increase in cloudiness and change in circulation during the selected forecast period. The March case study presented in Section IV was selected for analysis because it was

representative of several good examples where the information contained in the sequences of ATS photos significantly augmented conventional data.

In addition, examination of these data has provided some insight for possible future application of this model into ATS type data for the numerical prediction of clouds, precipitation and circulation. (Section IV)

B. Compensation and Clouds

The concept of compensation is offered as a key to understanding and predicting the appearance of satellite photographs, especially those over large areas such as ATS photographs. In the tropics and subtropics where conventional weather models (such as the wave cyclone) are not applicable, the compensation model is useful.

For the purpose of explaining this model, the condition is accepted that low level flow under a trade or other tropical inversion is very constant and very persistent compared to the upper level flow. Most of the time the inversion rises or falls slightly to allow compensation for upper air pressure changes and thus leaves the lower flow undisturbed. This process is the source of the term.

If the inversion height over the lower moist layer is near the condensation level, or if cloud heights can be determined, then the changes in height of the inversion will be indicated by clouds.

Some cloud patterns to be expected with traditional flows are shown in Figures 1-4. Easterlies with no upper air disturbance and light upper wind could have the inversion getting higher to the north as indicated in Figure 1. Arrows show upper wind, barbs show surface wind. The pattern with an upper air trough would indicate that the inversion rises slightly to keep the trough from showing up in the surface flow. This is shown in Figure 2, which gives an indication of the expected cloud pattern.

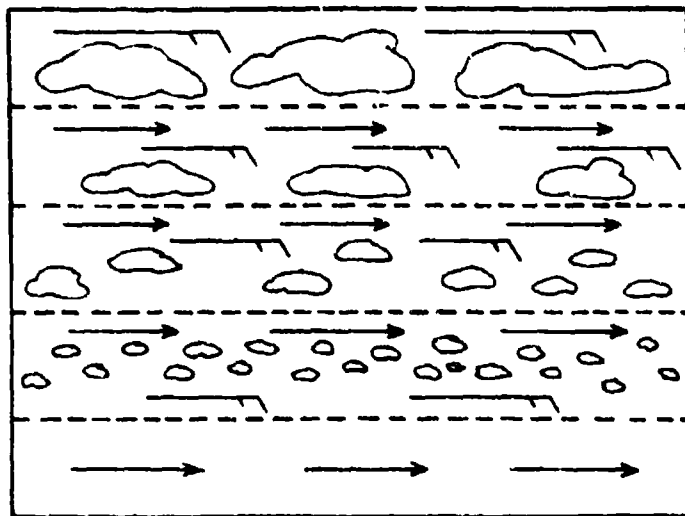


Figure 1. Easterlies with no upper air disturbance and light upper wind will have higher inversion in the north. High inversion height is shown by thicker cloud

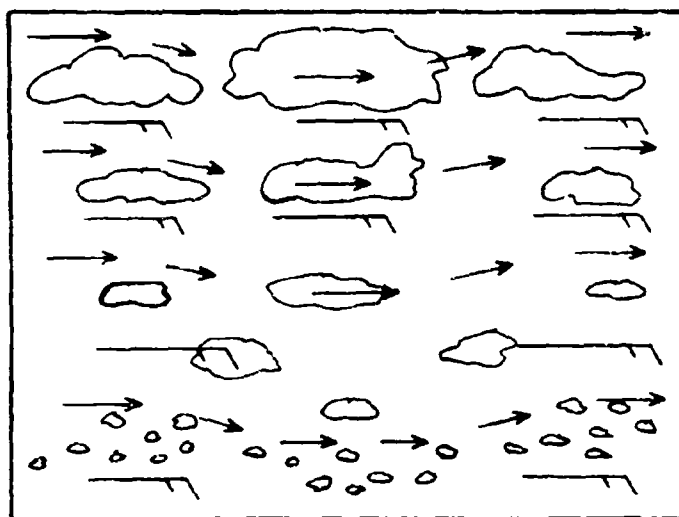


Figure 2. Upper air trough causes inversion to rise with little effect on surface flow. High inversion height is shown by thicker clouds.

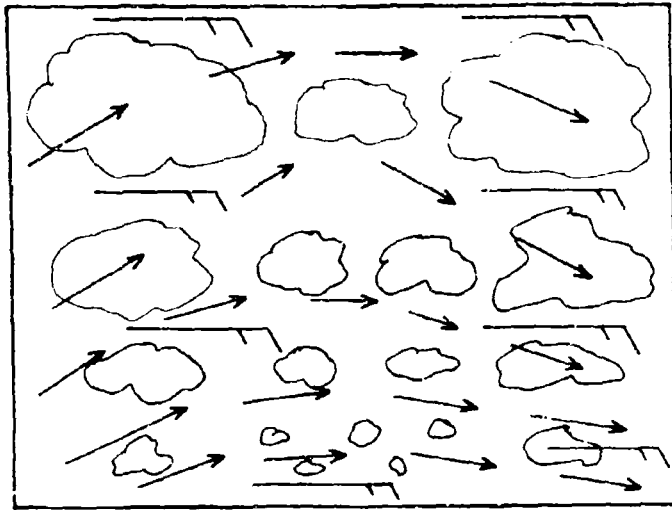


Figure 3. Upper air ridge causes inversion to lower suppressed clouds. Higher inversion height is shown by thicker clouds.

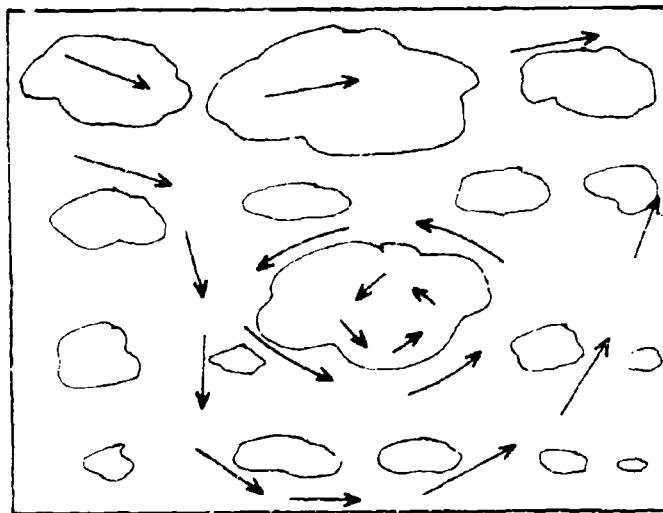


Figure 4. Upper air low cell causes inversion similar to trough, with modification as shown. Higher inversion heights are shown by thicker clouds.

An upper air ridge would cause the inversion to get lower and would suppress the clouds as in Figure 3. An upper air low cell would be similar to a trough, but with some modification, as shown in Figure 4. There would be a similar modification for a high cell. These patterns would be particularly meaningful if the satellite photographs were watched daily and changes noted. For example, Figure 5b would indicate a trough and Figure 5c would indicate a ridge over the area which originally looked like 5a.

To summarize, compensation is a slight adjustment of the inversion height to compensate for upper air pressure changes and leave the flow below the inversion relatively undisturbed. Response in the form of height change is small, and vorticity changes in the lower layer are usually negligible.

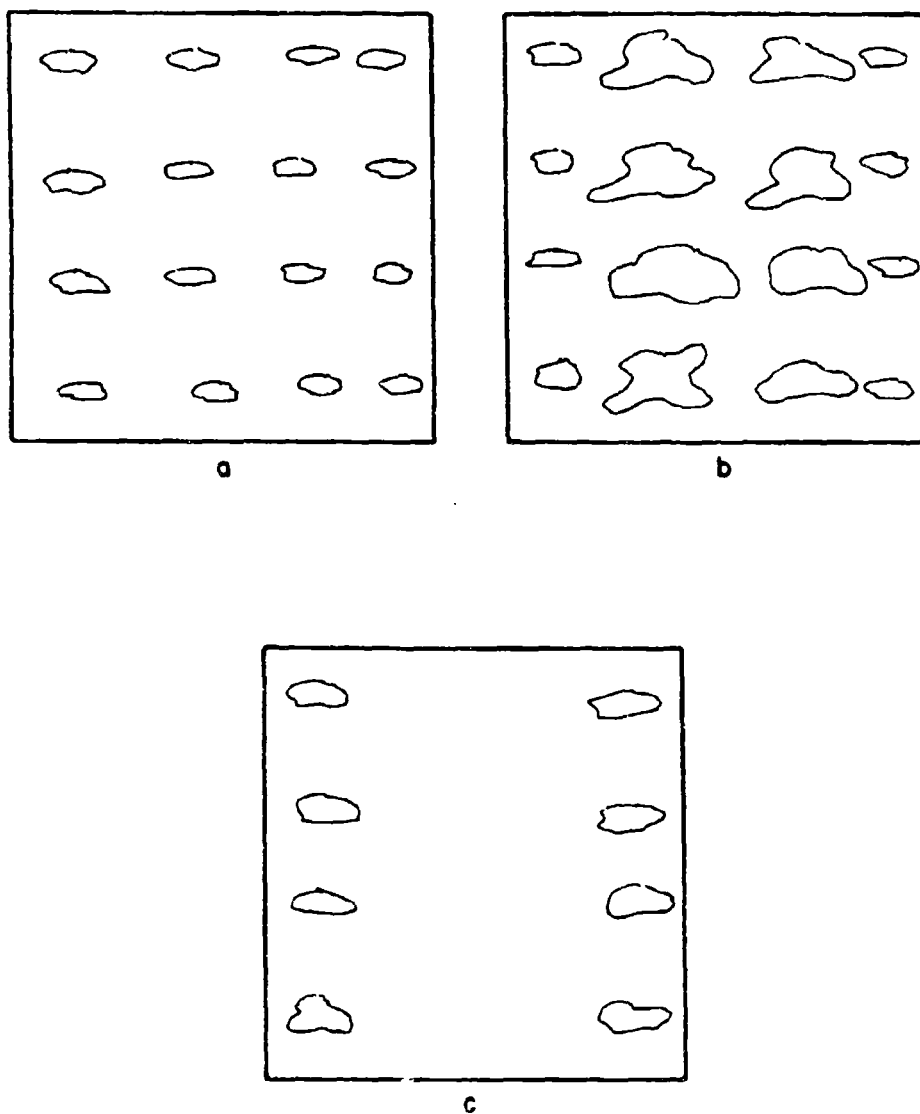


Figure 5. Prediction of inversion from satellite photographs. b. would indicate a trough, or c. would indicate a ridge, over area previously like a. That is, higher inversion heights are shown by thicker clouds.

C. Moist Overcompensation

When clouds form in a moist layer forming an inversion below a dry layer there is a built-in mechanism for weakening the inversion. As the air rises the saturated lower air cools with the moist adiabatic lapse rate. If the air continues to rise the inversion will eventually disappear. This mechanism, coupled with the compensation mechanism, leads to moist overcompensation. When the height required for compensation is so great that the inversion must exceed the level at which the inversion is dissipated, then moist overcompensation results.

Formation of clouds means that increased inversion height becomes less and less effective in causing compensating pressure changes. Decreasing pressures aloft can only be compensated by extraordinarily high inversion heights, resulting in thick clouds and possible measurable changes in the vertical component of the vorticity. In extreme cases all stability is eliminated. It finally becomes impossible for the surface pressure pattern to differ from the upper air pressure pattern and the surface flow comes under the influence of strong pressure gradients from aloft.

This phenomenon can best be illustrated by describing the flow in the easterlies under a deepening upper air trough. In Figures 6, 7, 8, 9, and 10 we have plotted contours of the inversion height, upper air winds and surface winds.

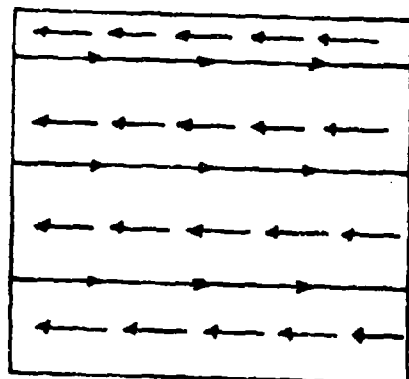


Figure 6. Schematic representation of undisturbed subtropical easterly flow underlying upper level westerlies. Upper level westerlies superimposed on inversion height contour lines.

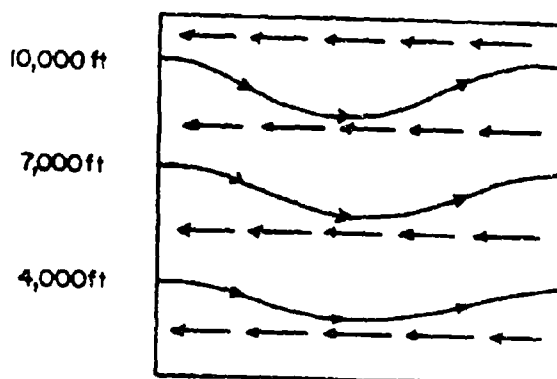


Figure 7. Illustration of compensation by upward adjustment of inversion height for a disturbance in the upper westerlies so that low level easterlies are maintained.

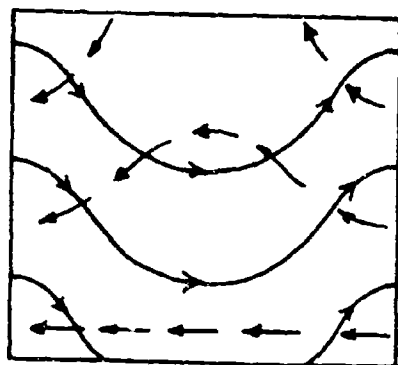


Figure 8. Illustration of the case where compensation cannot maintain the low level easterly flow, and the high level perturbation is reflected at the surface.

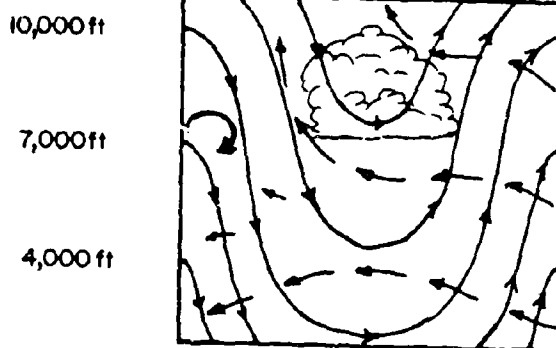


Figure 9. Evolution of low level flow and cloud patterns subsequent to Figure 8. Inversion has been destroyed in cloud area. In all drawings the inversion contours are almost parallel to the upper winds.

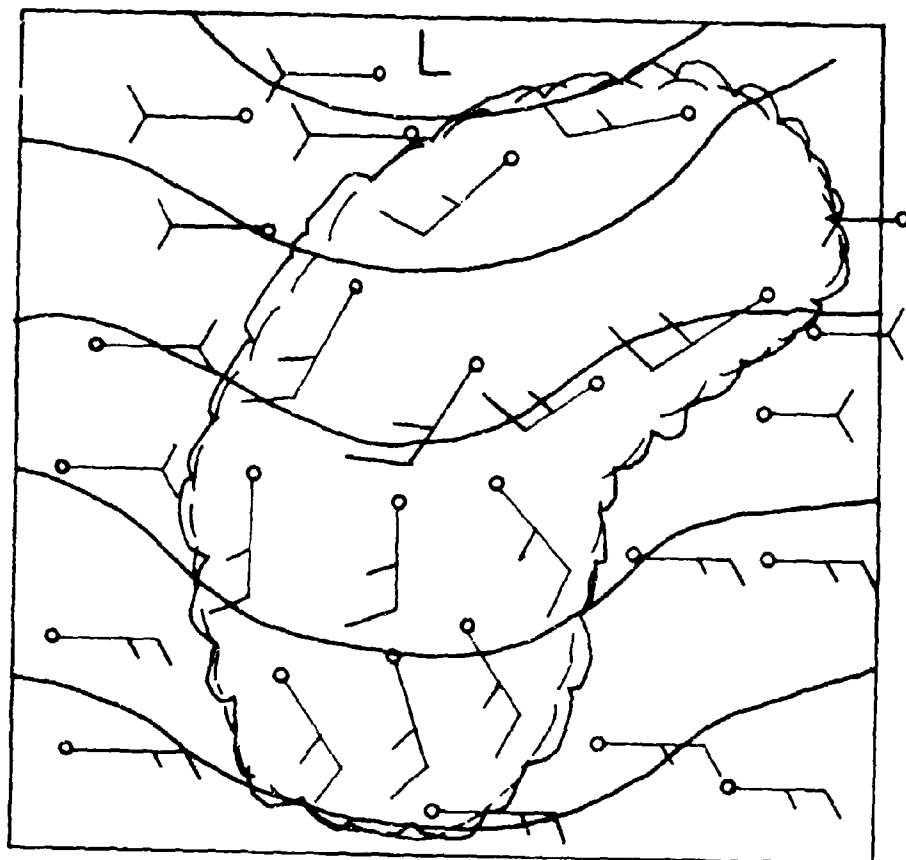


Figure 10. Large scale moist overcompensation leads to the upper air pressure gradient causing "geostrophic" west winds at the surface.

Figure 6 shows the straight westerly flow over the straight easterly flow, with the inversion sloping to compensate for the difference between flows. The low pressure in the upper trough in Figure 7 is compensated by the increase in inversion height so the east winds continue in the lower levels undisturbed. In Figure 8 the trough has become so strong that the compensating effect has lifted the air so high the clouds formed have reduced gravitational stability to almost nothing. Finally, it is no longer possible to compensate and the upper air pressure gradient cannot be shielded from the surface air. Figure 9 illustrates a strong south wind resulting from acceleration of the surface air by the upper air pressure gradient that accompanies west winds aloft.

If this event occurs on a large enough scale so that geostrophic balance is expected, then we have west winds at the ground as shown in Figure 10 .

On a smaller space scale or a shorter time scale it would be expected that the air moving into the cloudy area under west winds aloft would move to the north (Figure 9). This northward moving air is not necessarily confined to the surface layers, so it can continue to rise and become a plume of clouds at high levels streaking from southwest to northeast.

D. Moist Air Injection

Occasionally the southerly (or subtropical) core of the jet stream undulates equatorward over the moist easterlies, and causes moist overcompensation. When the ability for compensation is exhausted the warm moist air rises and pushes up the tropopause, causing an increased tropopause height over a large area. This increased height starts two waves on the tropopause, one streaming off to the southeast and one streaming off to the northeast. The wave streaming off to the southeast is lost in the equatorial cloudiness but the one moving off to the northeast becomes a streak of moist air and cloud--and highly visible on satellite photographs (see streak off west coast of Baja California in Figure 20).

The northwest side of this injection can be in geostrophic balance and may not contribute to the northward advance of the wave, but the southeast side cannot be in geostrophic balance with southwest winds so the advance of the tropopause wave would be expected to have a peak behind it. (Figure 11).

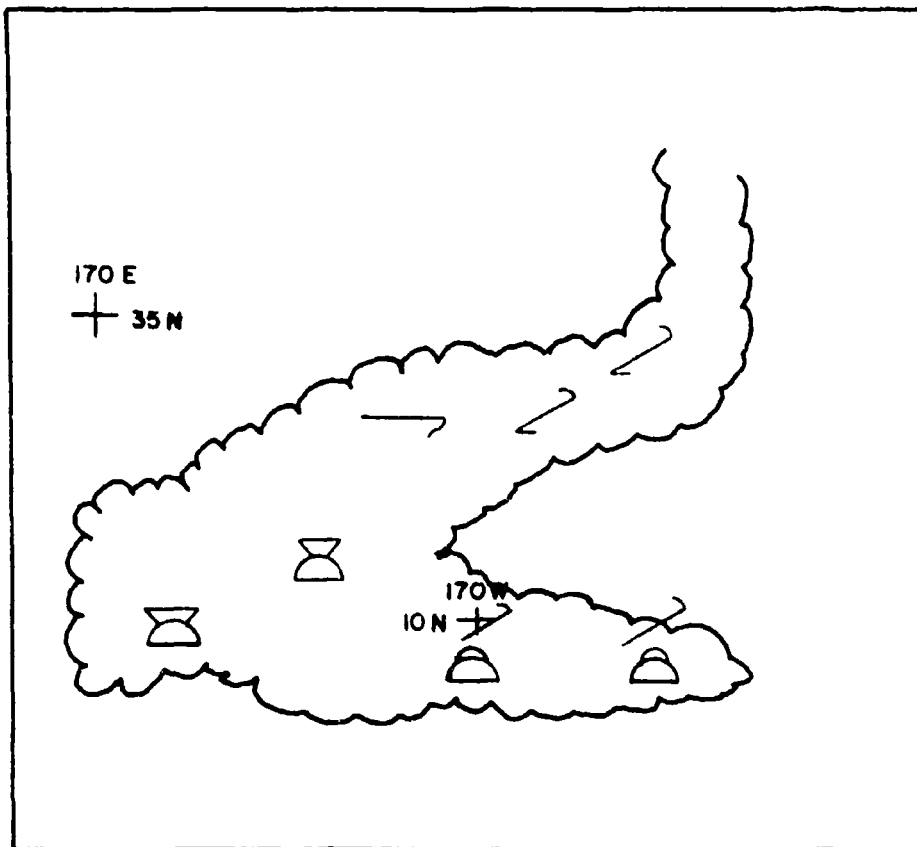


Figure 11. High level cloud streaming out of the tropics.

F. Theory of Moisture Influx

The source of moisture in the air is nearly always considered to be near the ground. In order to simulate this concept (which is also backed by adequate observation) we assume that there is a layer near the ground with gravitational stability and a high relative humidity (50-70%). When this moist layer is lifted enough that the relative humidity becomes 100%, clouds form, and the lifting lapse rate in the low level air becomes the saturated adiabatic. Then if the upper air is lifted, following the dry adiabatic rate, the net result is a decrease in gravitational stability. Repetition of this process leads to less and less stability, enabling the clouds to move very rapidly up to the tropopause where the stability again becomes very large.

The particular formulation of the problem developed here is based on gravitational stability in the rising air. This was done primarily for convenience of computing, but there is some basis for it in certain large circulation patterns where complete instability (warm moist air under cool dry air) is not likely. A large, absolutely flat, unstable region would allow cooler dry air to fall into the moist air, and the resulting cooler moist air might then be stable. See Figure 12. The arrangement in (a) is not likely. But if the large flat area of cold air is unstable, so that the cold air intrudes downward, it will cause a picture similar to (b), a stage (perhaps not observed) in the mixing of cool upper air into a large area of saturated moist

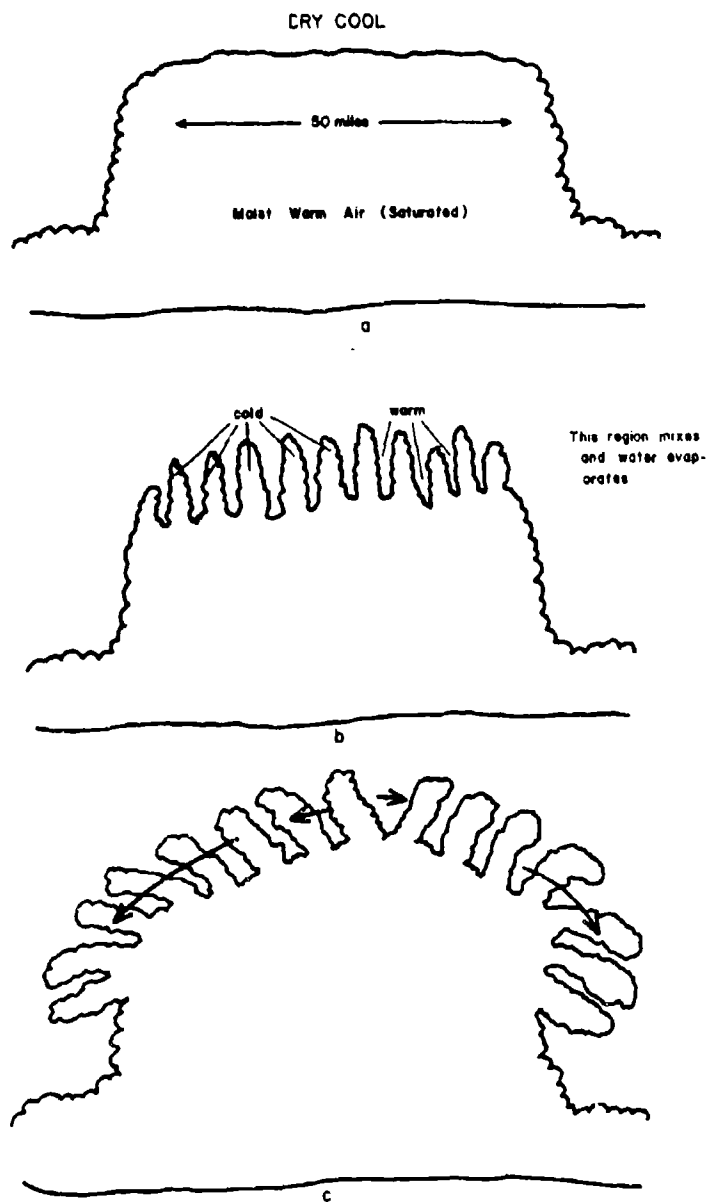


Figure 12. Stages in a rising large scale cloud mass.

air. The actual picture is probably more like (c), which implies mixing of the rising warm air and dry air above, with the cool mixed air flowing downward on the edges.

F. Introduction of Moisture Into the Prediction Model

The study of the effect of moisture on the flow is carried out with the following system of equations. We define the symbols below:

θ — potential temperature below inversion in degrees Celcius

θ' — potential temperature above inversion in degrees Celcius

$\Delta\theta$ — difference in temperature across the inversion at condensation level in Celcius degrees

h_c — the condensation level in miles

H — height of the tropopause (approx. 40,000 ft.) in miles

Γ_1 — upper constant of stability in mi/hr^2

h_m — maximum gravitational stability height in miles

h — height of inversion above sea level in miles

h_g — height of ground surface above sea level in miles

Compute: h_m

Note h_m here is the maximum height for gravitational stability; the low level air is cooler than the upper level air when h is less than h_m .

From $\Delta\theta - 7.2(h_m - h_c) = 0$ obtain $h_m = \Delta\theta/7.2 + h_c$. The input parameters are assumed to satisfy the conditions:

$$\Delta\theta \geq 0 \text{ and } H \geq h_m.$$

Figure 13 illustrates temperature distribution. The conversion factor used is 1.8. There are four cases:

$$\text{Case I} \quad h < h_c \quad \gamma = \frac{\Delta\theta}{\theta} g$$

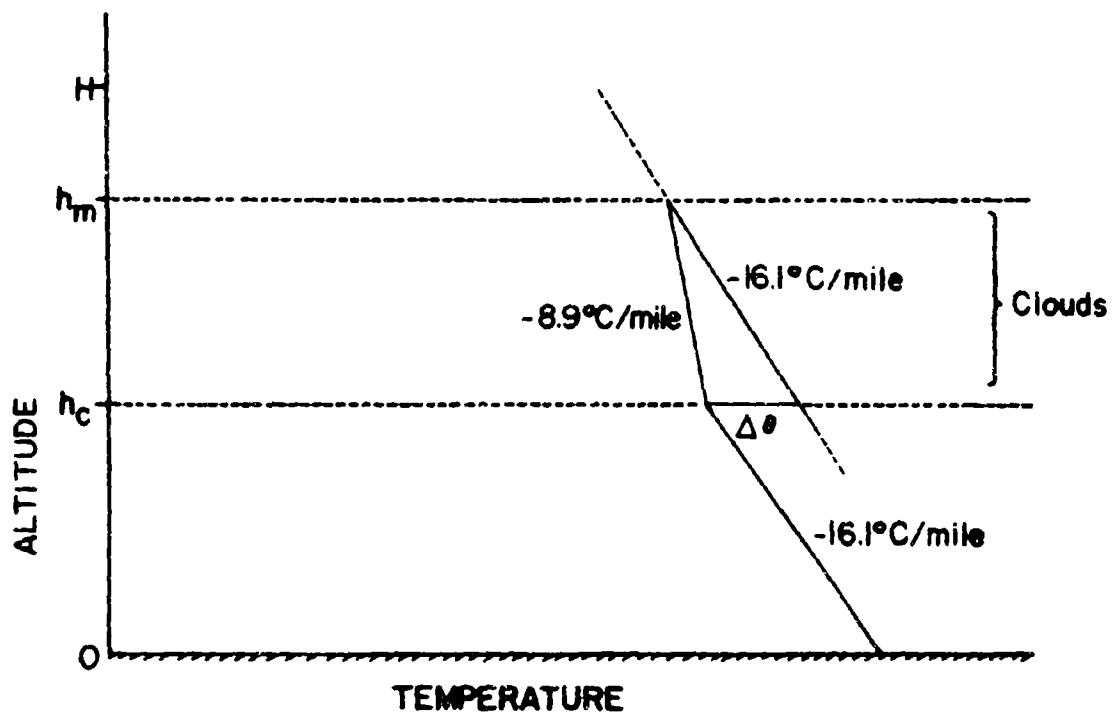


Figure 14. Temperature distribution in dry air and in clouds.

Case II	$h_c \leq h < h_m$	$\gamma = \frac{\Delta\theta - 7.2(h-h_c)}{\theta} g$
Case III	$h_m \leq h \leq H$	$\gamma = 0.1 \frac{\Delta\theta}{\theta} g$
Case IV	$H < h$	$\gamma = \Gamma_1$

When there is no cloud, and air above and below the inversion is following the dry adiabatic law, we have Case I, ($h < h_c$) with the equations

$$\gamma = \frac{\Delta\theta}{\theta} g$$

$$\frac{\partial u}{\partial t} + u \frac{\partial u}{\partial x} + v \frac{\partial u}{\partial y} = -\gamma \frac{\partial h}{\partial x} + f(v - v') - ku\sqrt{u^2 + v^2} \quad (1)$$

$$\frac{\partial v}{\partial t} + u \frac{\partial v}{\partial x} + v \frac{\partial v}{\partial y} = -\gamma \frac{\partial h}{\partial y} - f(u - u') - kv\sqrt{u^2 + v^2}$$

$$\frac{\partial}{\partial t}(h - h_g) + \frac{\partial}{\partial x} \left[u(h - h_g) \right] + \frac{\partial}{\partial y} \left[v(h - h_g) \right] = 0$$

In these equations u, v are wind components in the lower air. u', v' are the wind components in the upper air. h_g is the height of the ground surface above sea level; k is the drag coefficient of the ground. Cloud formation is associated with a higher and a weaker inversion. This is illustrated by Case II, ($h_c \leq h < h_m$) with Equation (1).

When the inversion height reaches h_m , assume that γ is constant in the region between the maximum height for gravitational

stability, h_m , and the tropopause height H , and we have Case III, ($h_m \leq h \leq H$) with Equation (1). This small amount of stability takes into account the cooling and mixing of the moist air with the upper air by maintaining the stability.

When the surface air reaches the tropopause we have a very stable deep layer that follows the equations in Case IV, ($h > H$) with Equation (1) but now with u' and $v' = 0$.

In each of the above cases the inversion level winds u' and v' are assumed to be functions of the inversion height h . The functions $u'(h)$ and $v'(h)$ are defined so as to approximate the ambient thermal winds between the low level inversion and the tropopause. The functions u' and v' could be defined as $u'(x, y, t, h)$ and $v'(x, y, t, h)$. For this particular program they were defined as $u'(h)$ and $v'(h)$.

II. THE SYNOPTIC SITUATION FOR THE PREDICTION EXPERIMENT

Keith Veigas and Pieter Feteris

A. Procedure

The map and ATS photo series for 6-10 April 1967 were selected for initial prediction experiments employing the model described in section I of this report. As all meteorological maps are marked Z for GMT, this notation has been used for consistency and brevity.

Figures 14, 15, and 16 for 7 April 1967 illustrate the initial conditions for the first prediction experiment. Figure 14 shows the surface chart for 0000Z, and the associated ATS photocommencing approximately 2 hours prior at around 2217Z 6 April.

The shaded area on the surface chart (Figure 14) is the prediction area. The low level flow is predominately easterly and the ATS photo coupled with available surface observations indicate only very widely scattered areas of convective activity.

Circulation in the middle and upper troposphere at 0000Z 7 April are shown on Figures 15 and 16. There is an upper level vortex centered over the western boundary of the prediction area, with southwesterly winds at 500 mb over the low level easterlies and predominately westerly flow in the upper troposphere.

Approximately 24 hours later the ATS photo commencing at 2340Z 7 April and reproduced in Figure 17 indicates a considerable difference in the cloudiness and associated moisture distributions. Also included

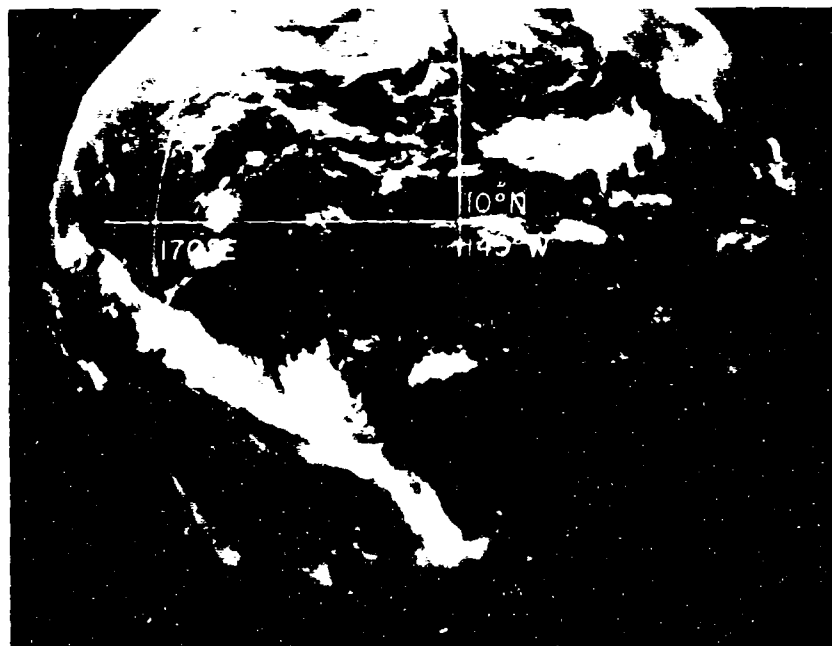
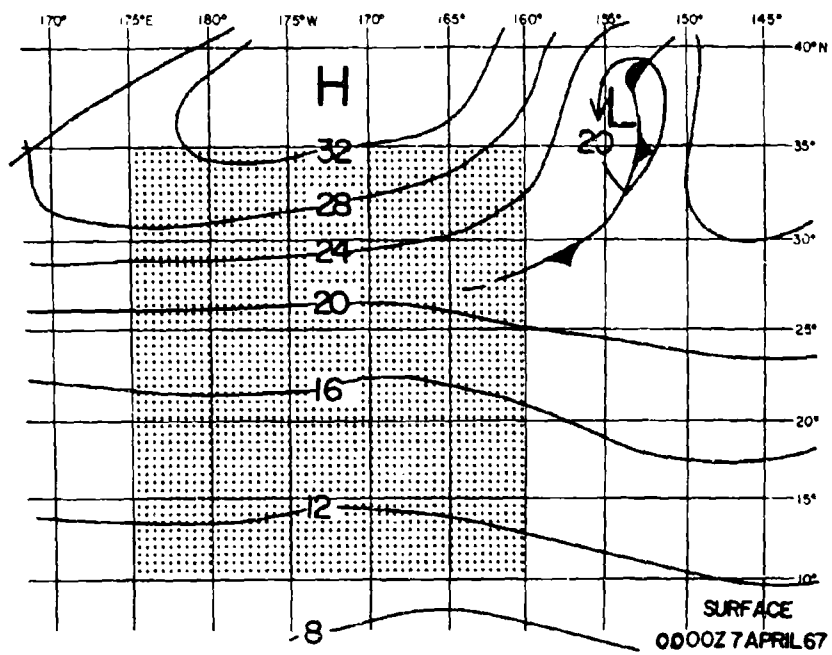


Figure 14. Surface chart for 0000Z 7 April and ATS photo for 2217Z 6 April 1967.

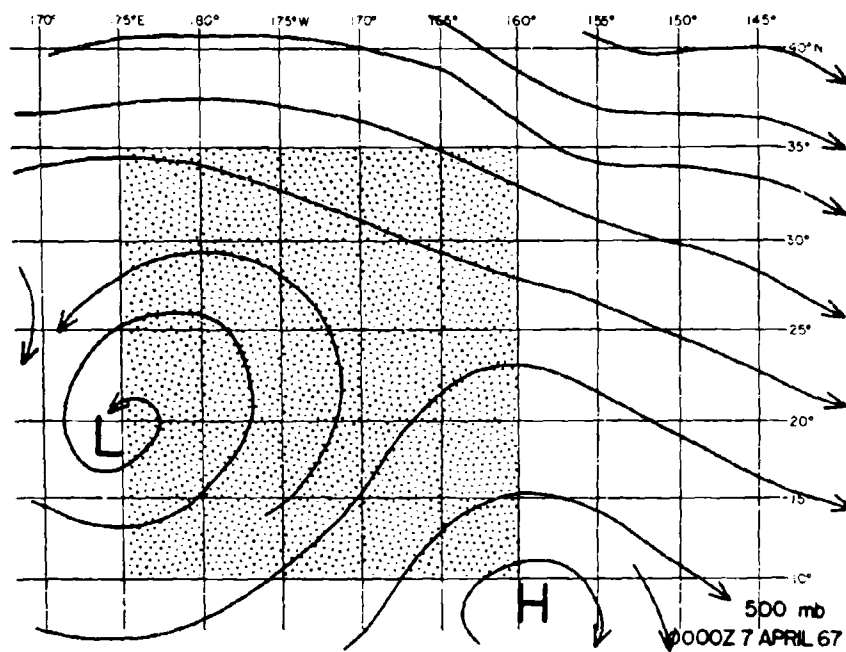


Figure 15. 500 mb streamline analysis chart for 0000Z 7 April 1967.

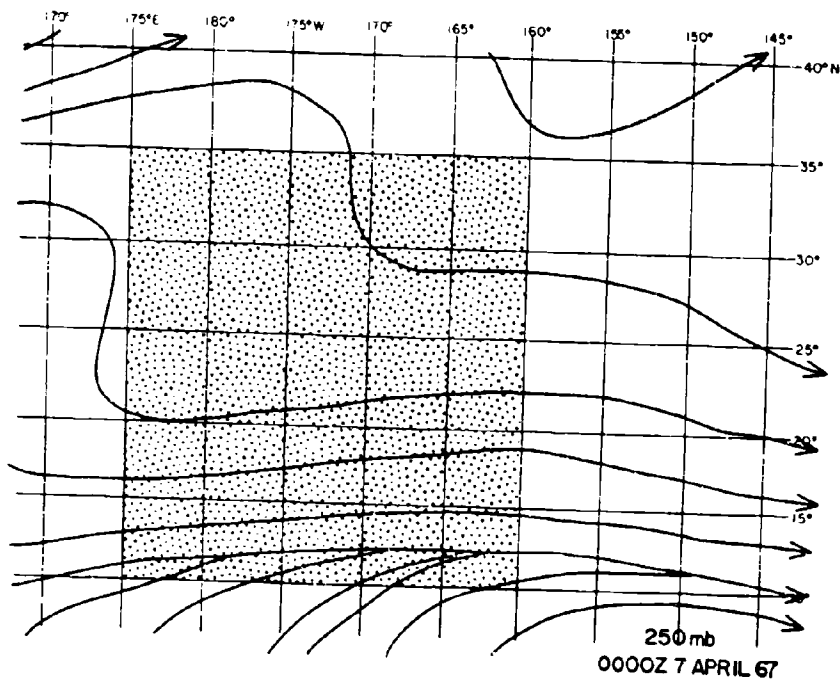


Figure 16. 250 mb streamline analysis chart for 0000Z 7 April 1967.

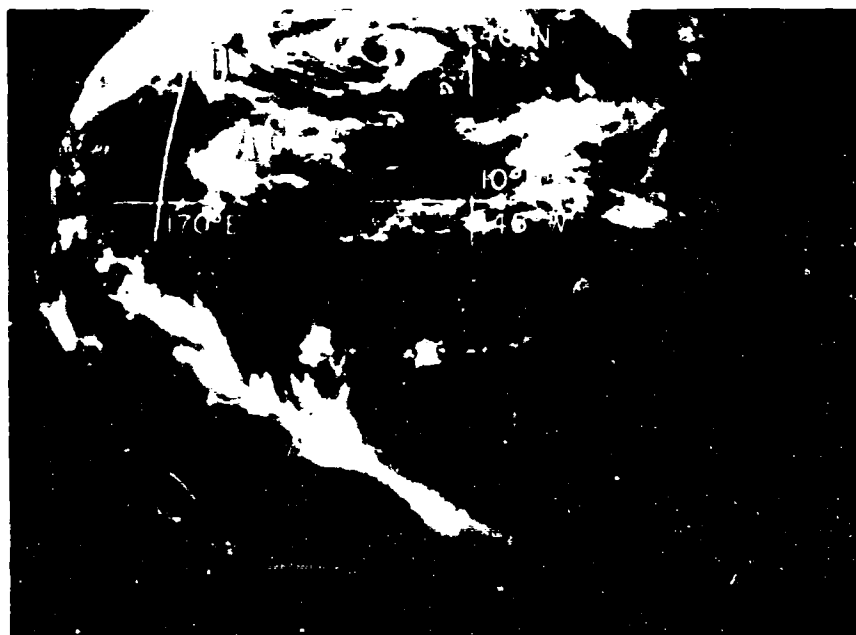
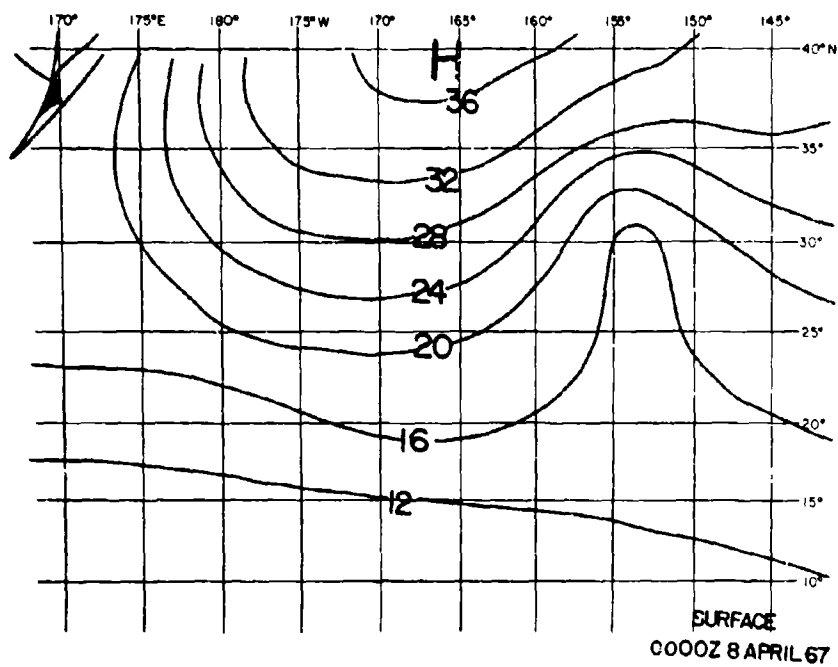


Figure 17. Surface chart for 0000Z 8 April and ATS photo for 2340Z 7 April 1967.

in Figure 17 is the surface chart for 0000Z 8 April. A plot of conventional cloud observations on this day indicates that the cloudy area labeled A on the ATS photo is marked by much more widespread deep convection than on the previous day. The flow in the lower layers to the south and east of Hawaii is still predominantly from the east. In the mid-troposphere it can be noted that a cyclonic vortex remains in the western section of the region of interest, and the associated southerly flow that has developed in the mid-tropospheric regions (Figures 18 and 19) is still not reflected in the lower layers of the atmosphere. Qualitatively, according to the arguments of Freeman (Section I), this should lead to an increase in the depth of the zone of the easterlies from Hawaii toward the center of the mid-tropospheric vortex. An increase in the depth of the easterlies implies upward vertical motion and eventual release of convective instability. This can lead to condensation in the moist lower layer, leading to the development of vigorous convective action which will "break" the cap of the inversion and the development of moist areas through rather deep layers of the troposphere. A deep moist layer can subsequently be injected into midlatitude weather systems. An evolving pattern of this type is indicated in Figures 20 and 21 of the ATS photos late on the 8th and 9th of April.

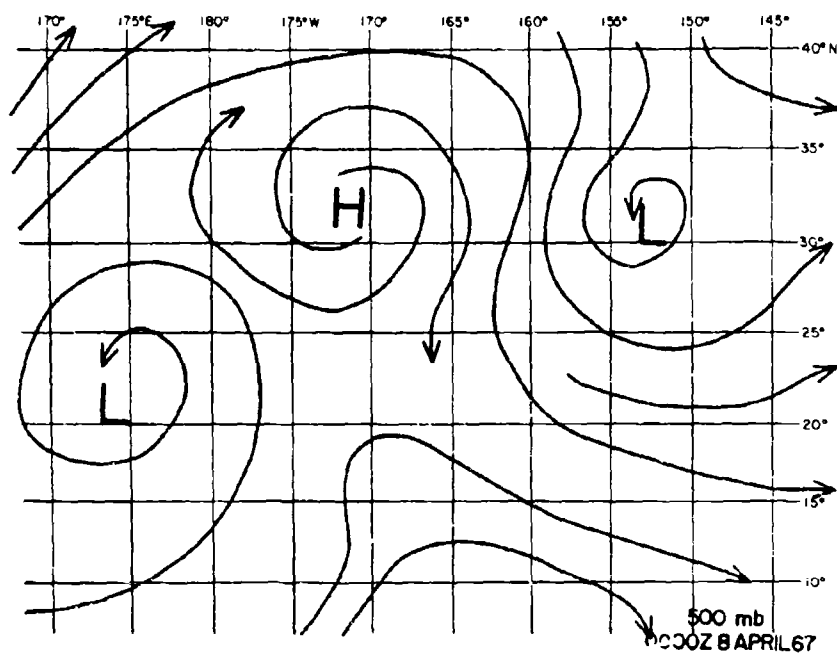


Figure 18. 500 mb streamline analysis chart for 0000Z 8 April 1967.

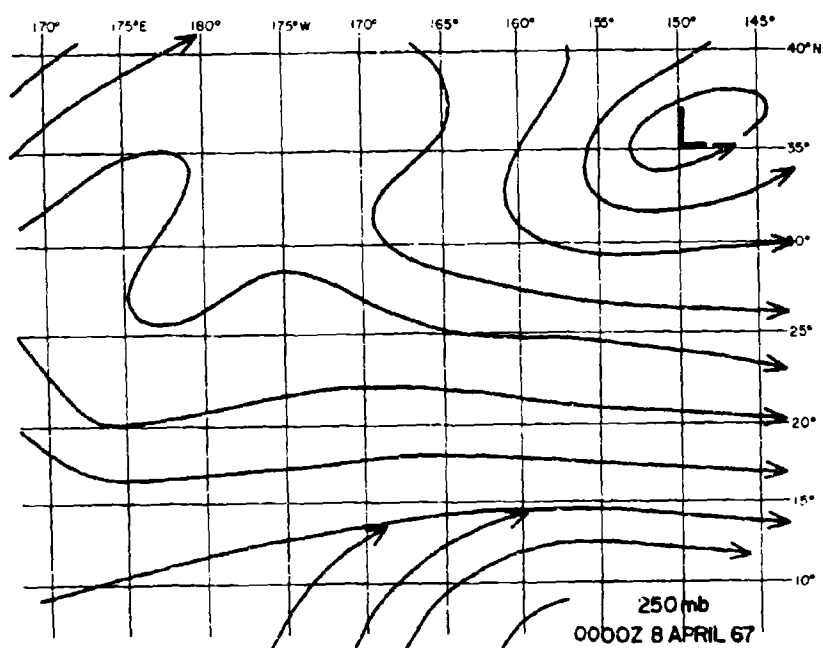


Figure 19 250 mb streamline analysis for 0000Z 8 April 1967 .

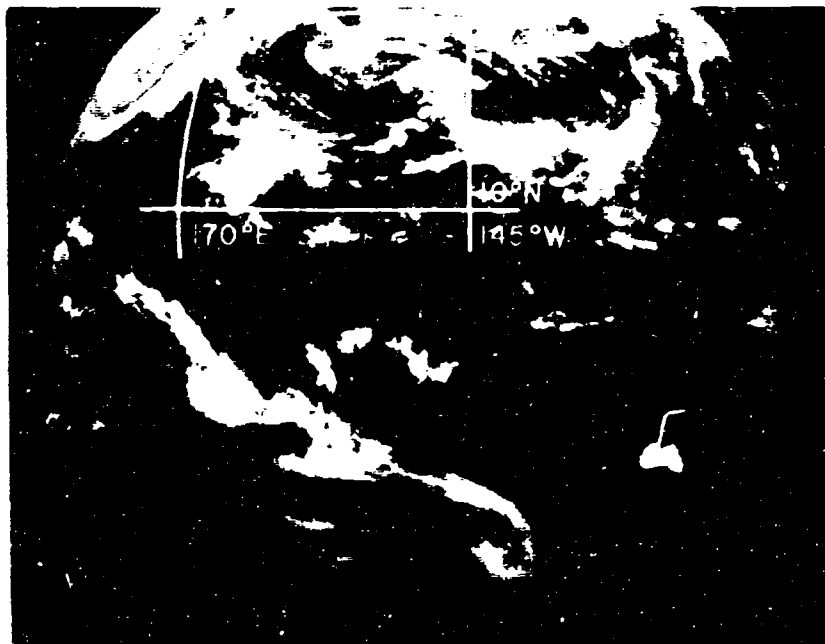


Figure 20. ATS photo for 2223Z 8 April 1967.

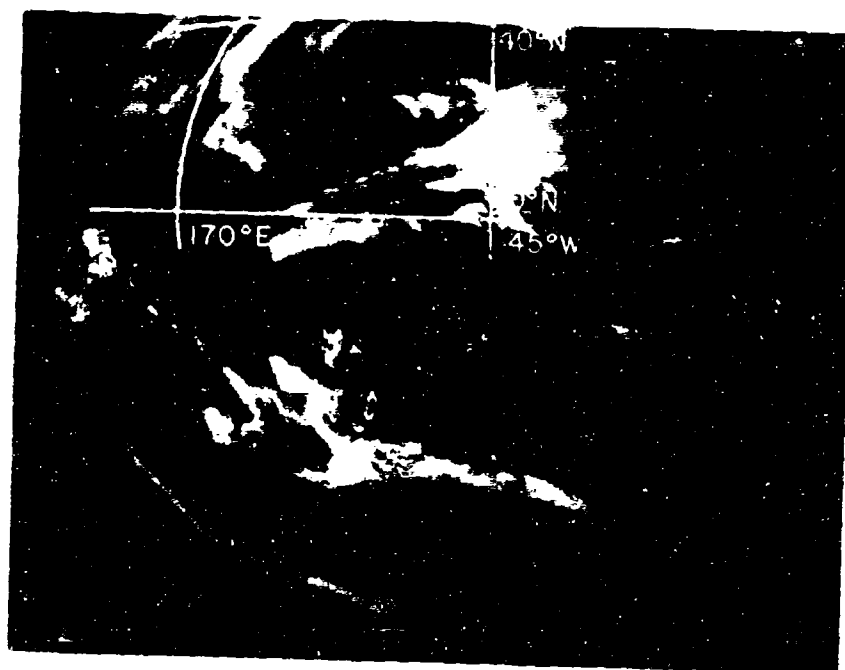


Figure 21. ATS photo for 2251Z 9 April 1967.

III. RESULTS OF THE NUMERICAL PREDICTION EXPERIMENTS

Keith Veigas and Sam Rosenberg

As indicated in section II of this report the weather satellite sequence commencing 0000Z 7 April 1967 was selected for our initial prediction experiments.

The important features of the synoptic situation, as revealed by the ATS photograph and associated synoptic charts shown in Figures 14, 15 and 16, are a broad belt of low level easterly winds, only widely scattered convective activity, and a middle and upper tropospheric disturbance at the western border of the prediction area.

Two prediction experiments were carried out. The height of the zone of the easterlies was assumed to be everywhere equal to one mile; in the first experiment $\Delta\theta$, strength of the inversion, was designated 3°C and in the second 6°C .

The upper boundary conditions and those at the periphery of the grid were held constant, which limited the prediction period to six hours.

Estimates of the T_0 winds were based on analyses prepared by the ESSA Weather Bureau in Honolulu. Analyses were available for the surface, 700, 500, and 250 mb levels. The components of the T_0 low level wind field are shown in Figures 22 and 23.

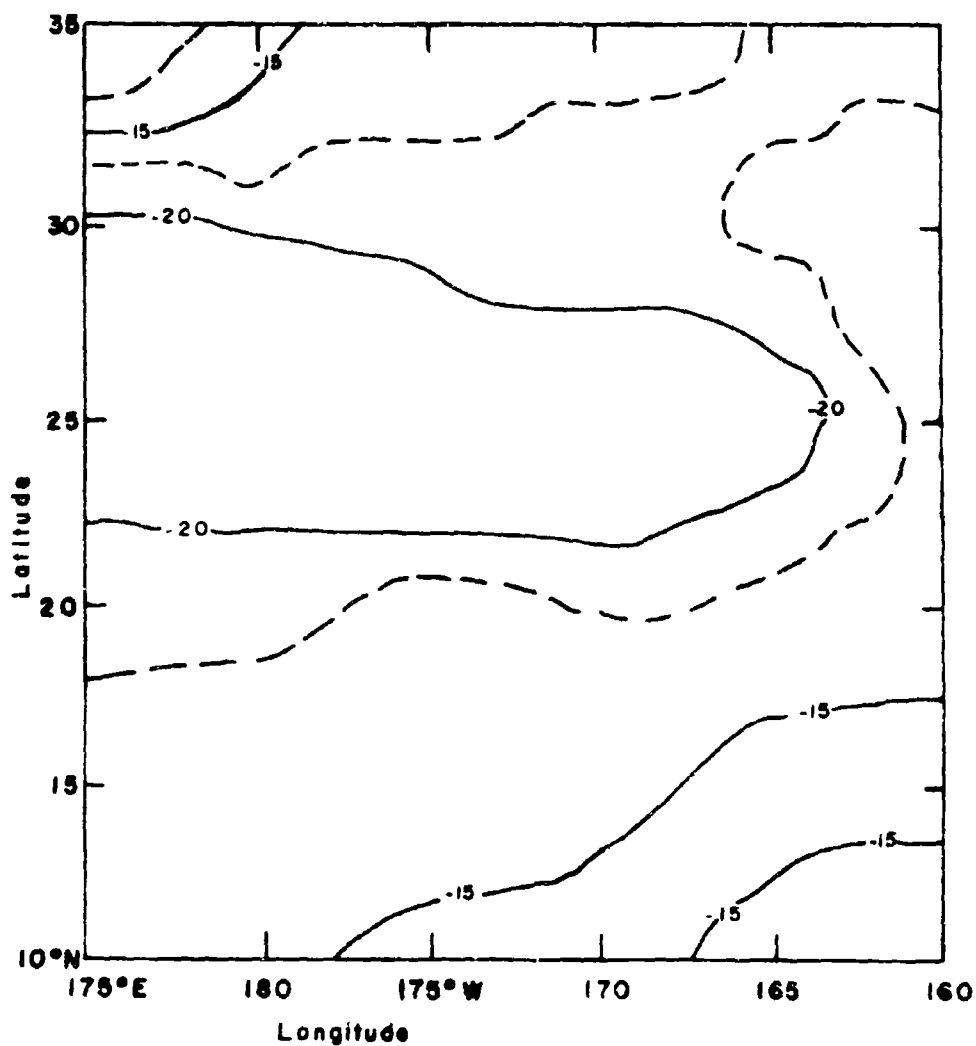


Figure 22. Map of observed u component of the low level wind field (in knots) for 0000Z 7 April 1967.

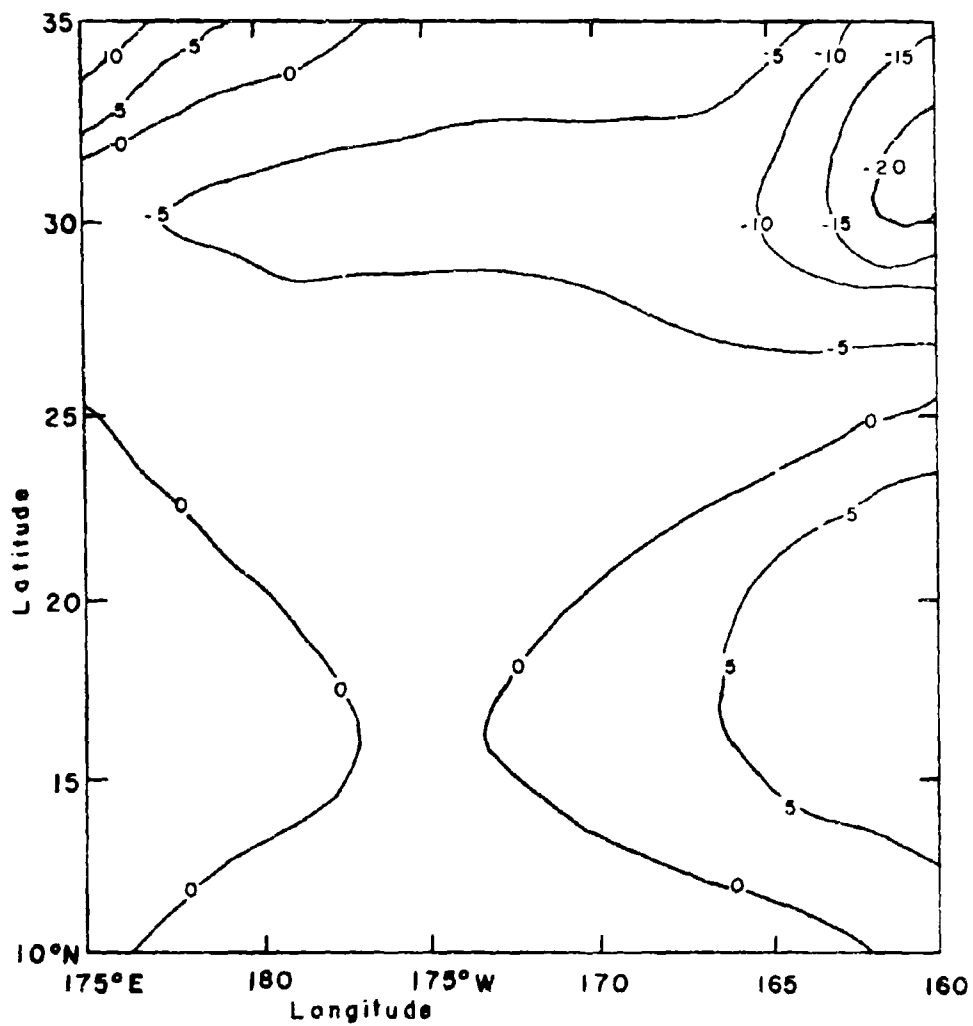


Figure 23. Map of observed v component of the low level wind field (in knots) for 0000Z 7 April 1967.

The components of the low level wind field at $t_0 + 6$ hours are shown in Figures 24 and 25. The u component exhibited only small changes, but a rather dramatic change in the v component from nearly zero to a strong southerly component was predicted. (This predicted change was realized (see Figure 17); however, the zone of increase of southerly winds was northwest of the predicted area of increase.)

The predicted change in height of the layer of the easterlies is shown in Figure 26 and there is a good correspondence between the area of implied upward vertical motion and the developing cloud areas as depicted by a subsequent ATS photograph (Figure 17) for 2340Z 7 April 1967. For example, see cloud areas labeled B, C, D, on the prognostic h chart and the ATS photograph. In each case the upward motion implied by the h prognostic chart corresponds quite well with the developing cloud areas.

Experiment II with $\Delta\theta$ set at 6°C produced results very similar to experiment I illustrated in Figures 24, 25, and 26. The predicted southerly components of the low level wind and the increases in the height of the low level patterns were slightly higher, but it can be concluded that the model is not highly sensitive to the specification of $\Delta\theta$. This is an important result in that only gross estimates of $\Delta\theta$ can be expected in the data sparse regions.

It is felt that future diagnostic-prediction studies, which are beyond the scope of this study, should include:

1. Introduction of time dependent boundary conditions from mid-

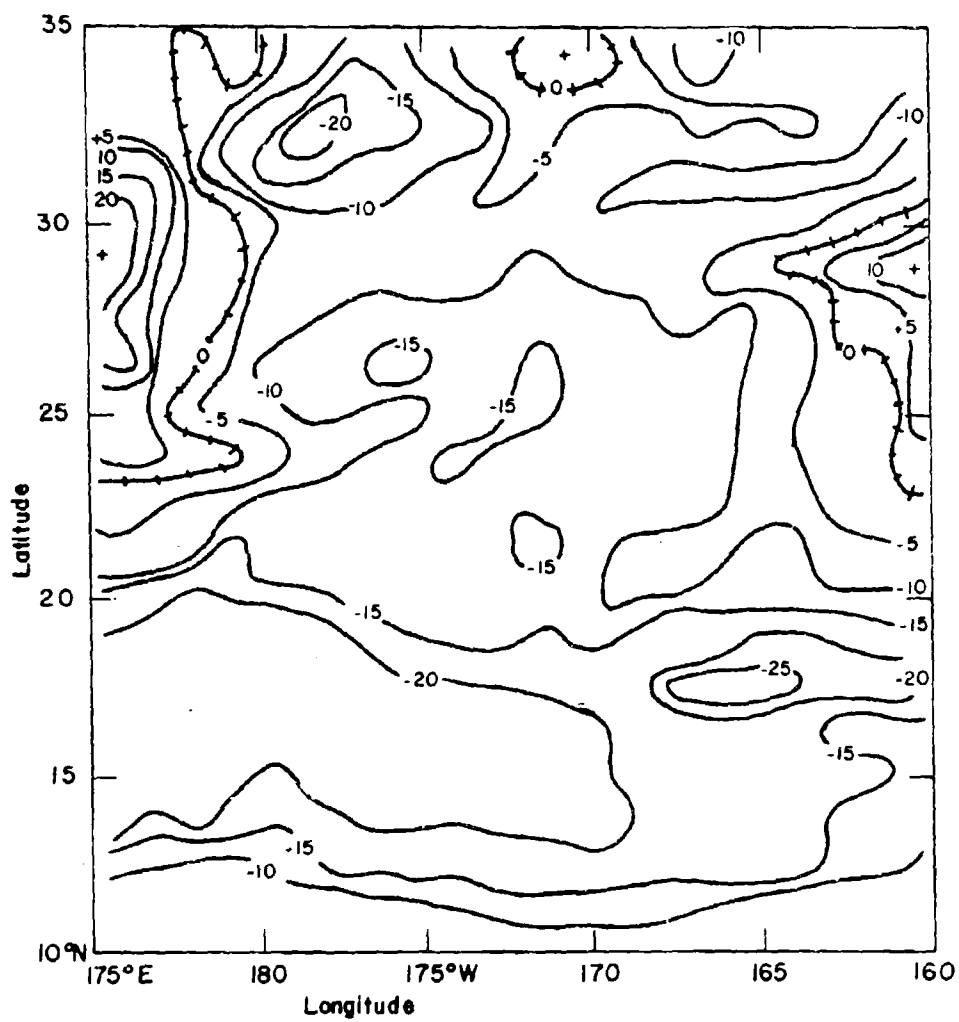


Figure 24. Map of predicted u component of low level wind field (in knots) for 0600Z 7 April 1967. ($T_0 + 6$)

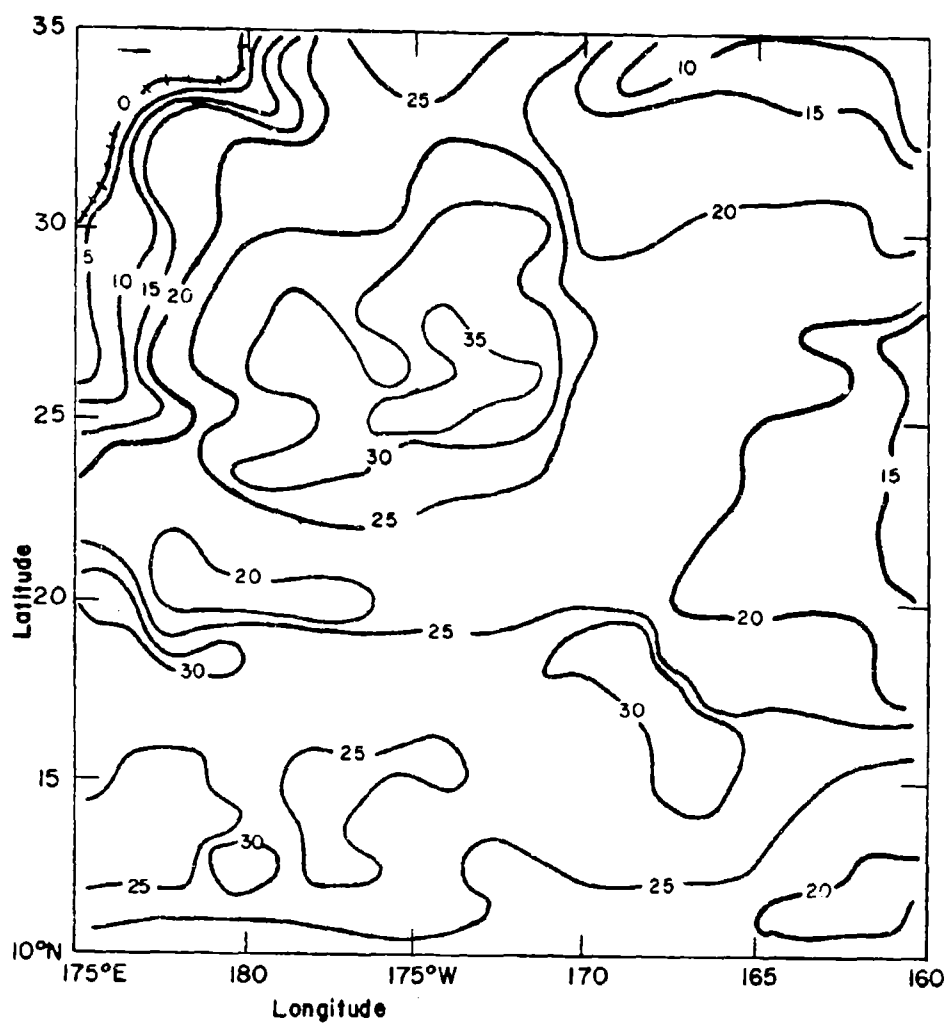


Figure 25. Map of predicted v component of the low level wind field (in knots) for 0600Z 7 April 1967. ($T_0 + 6$)

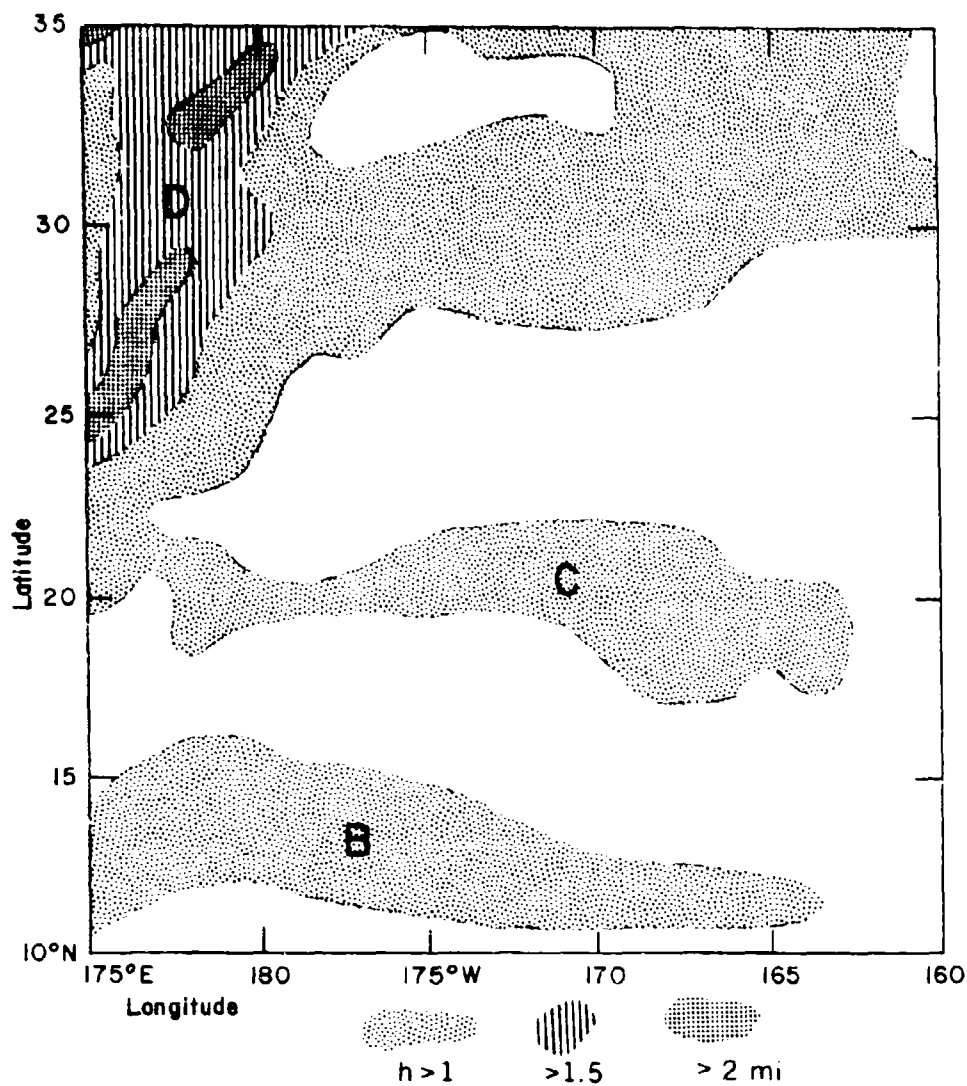


Figure 26. Map of predicted height (nautical miles) of the layer of the easterlies 0600Z 7 April 1967.

latitude numerical predictions where possible.

2. Introduction of effects of the release of latent heat of condensation from convective scale processes on the synoptic scale generation of kinetic energy.
3. Introduction of the flux of generated kinetic energy from low latitudes into mid-latitude prediction models.
4. Designing data archiving programs for satellite and conventional data, so that statistical "tuning" of this and other theoretical models is possible.
5. Utilizing special data collections, such as those anticipated in Project Bomex, to carry out more definitive prediction-diagnostic experiments.

IV. ON THE FUTURE USE OF ATS TYPE DATA IN NUMERICAL PREDICTION MODELS

Keith Velgas

A. Case Study

In the course of examining a series of weather maps and associated ATS photos in order to select test cases for the application of a dynamical prediction model for this study, several interesting situations were encountered which supply clues to ways in which ATS type information may be introduced into present and future "wet" numerical prediction models. In addition to the map series described in Section I, the series extending from 26 to 29 March 1967 is noteworthy.

Figure 27 shows the surface analysis for 0000Z 28 March 1967 and the associated ATS photo for 2252Z 27 March 1967. Note the cloud area B on the satellite photo and the surface chart. It is obvious from the conventional cloud observations that the cloud area represents a deep layer of moisture that has developed in the warm sector of the wave cyclone centered at about 39°N , 176°W longitude. The cyclone had been moving in a rather normal and consistent track, as indicated by the six hourly positions shown in Figure 27.

Figure 28 illustrates some rather dramatic changes in the cyclonic system. The surface analysis in Figure 28 is for 1800Z 28 March and the ATS photo is for 2137Z 28 March 1967. Judging from a careful analysis of the sequence of hourly surface charts there is good observational evidence

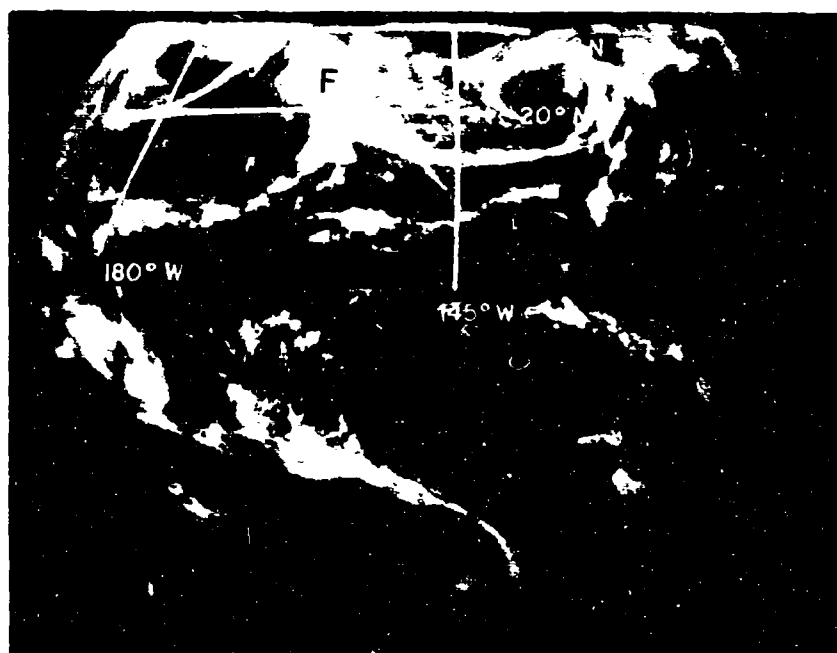
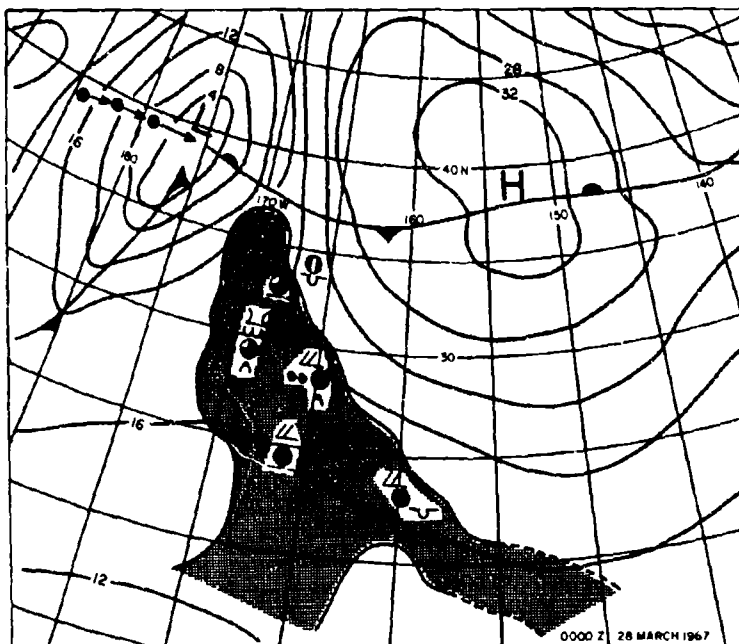


Figure 27. Surface chart for 0000Z 28 March and ATS photo for 2252Z 29 March 1967.

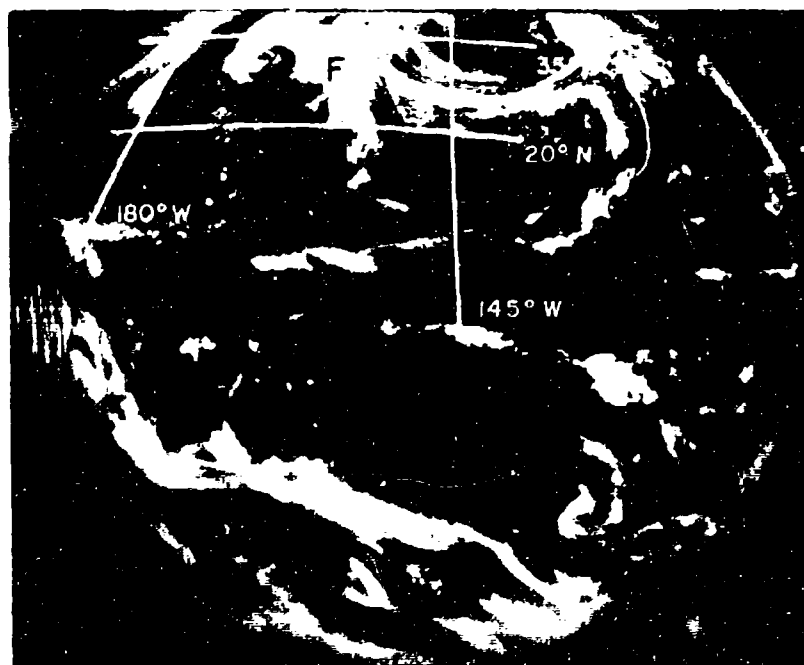
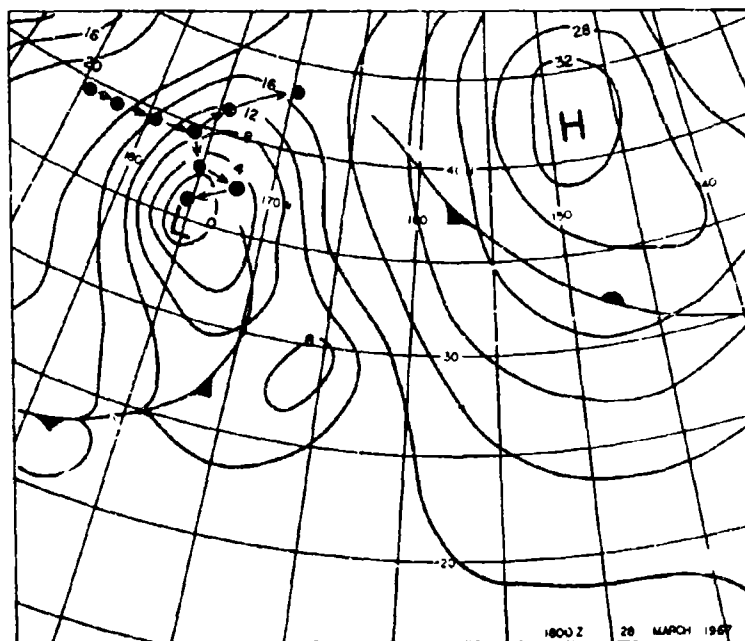


Figure 28. Surface chart for 1800Z 28 March and ATS photo for 2137Z 28 March 1967.

that the low cited in the previous figure split into two centers with the northernmost center moving to the ENE where it dissipated before the 1800Z 28 March map time. The southern center moved SE and deepened. An additional cyclone formed under the center of the deep moist layer indicated in Figure 27. Upon this new development the axis of these cyclones rotated in a counterclockwise manner.

In studying the sequence of events as depicted by the ATS and other satellite photos quite a different picture evolves. There is a noticeable shift to the south of the cloud mass associated with the cyclone centered about 40°N latitude at 0000Z 28 March, and the cloud area denoted by B in Figure 27 was injected into the midlatitude weather system. Thus it seems that utilizing satellite photos would likely have led to a better surface prediction in that it did indicate the tendency for the midlatitude weather system to shift to a more southerly course, and perhaps more importantly, the forecast of weather elements could likely have been improved with the knowledge of the spatial extent and direction of motion of a deep moist layer advancing into the weather system from the south.

B Use of Satellite Information in Numerical Weather Prediction

While useful information, i.e. circulation parameters, may be inferred from ATS type photos, additional useful information may be introduced in NWP cloud and precipitation models by the use of future ATS satellites. There is also increasing evidence that convective scale

release of latent heat in the tropics and subtropics must, in some manner, be taken into account in future prediction models.

The recent studies of hurricane development by Kuo (1965) and Miller (1969) clearly show that predicted behavior of forecast models depend very critically on the moisture content of the air. Blending of a variety of types of available information will be required to obtain the best possible estimates of moisture distributions over data sparse regions of the globe for input to future operation tropical and subtropical prediction models. It seems obvious from the ATS photos studied in the course of preparing for the numerical prediction experiments outlined in sections I and III of this report that ATS information can be extremely useful in delineating the spatial extent of vertical moisture distributions detected at points from conventional observation sources.

Prediction experiments should be designed to seek means of effectively incorporating this new source of information into operational and research prediction models, and further, to isolate the impact of improved initial moisture specification on the prediction of clouds, precipitation and circulation.

In addition it seems timely to suggest that the development of methods to combine various sources of humidity information should be accelerated. Chisholm, Ball, Velgas, and Luty, (1968) and Ball and Velgas, (1968) have shown that it is feasible to combine several types of humidity information to estimate free atmosphere humidity. They have further demonstrated that

these estimates lead to improved objective analysis of humidity distributions in data sparse regions.

The coupling of conventional and satellite information is a difficult problem, and much care must be exercised in developing techniques for inclusion of this new information into forecasting systems. This new information should be an invaluable adjunct to presently available information, as illustrated by Figure 29. The USAF AWS Global Weather Center kindly furnished us with their objective cloud analysis for the 0000Z 28 March 1967 study discussed above. The hatched area in Figure 29 is that area where the cloud amount was classified as indeterminate by the GWC analysis program because of lack of data. With the operational use of ATS satellites it is hoped that these "silent areas" will cease to exist.

In summary, these case studies have indicated that:

1. The use of satellite data to augment conventional observations will lead to more accurate estimates of moisture parameter for input to NWP models.
2. It became obvious that combining conventional and satellite data is not a trivial problem, because the different types of information vary in characteristics and accuracy.
3. Moisture inputs plus satellite-derived sounding inputs should yield much better specification of "wet" NWP model initial conditions.

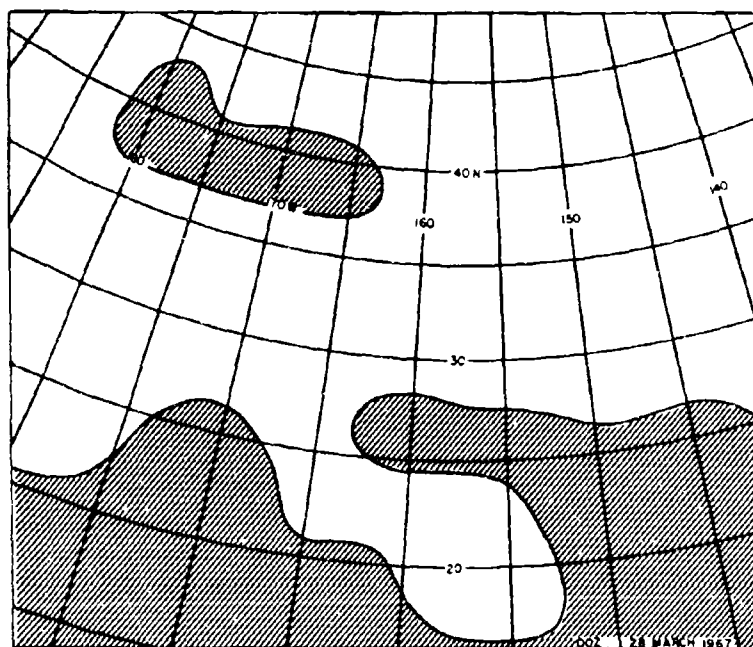


Figure 29. Hatched areas denote zones where conventional observations are inadequate to specify cloud cover on 0000Z 28 March 1967.

4. Definitive prediction experiments should now be designed to see if:
 - a. Improved cloud and precipitation predictions can be made.
 - b. Existing operational and research models can properly accommodate conversion of latent heat energy to kinetic energy in our circulation predictions.

REFERENCES

- Armijo, Larry, 1966: Statistical properties of radar echo patterns and the radar echo process. Technical Note 48- NSSL-27, National Engineering Science Company, Houston.
- Ball, J. T. and K. W. Veigas, 1968: The analysis of upper-level humidity. J. Appl. Meteorol., 7, 4, 620-625.
- Bomex Bulletin No. 4, prepared by The Bomex Project Office, May 1969.
- Chisholm, Donald A.; John T. Ball; Keith W. Veigas, and Paul V. Lutz, 1968: The diagnosis of upper-level humidity. J. Appl. Meteorol., 7, 4, 613-619.
- Kessler, Edwin III; and John A. Russo, Jr., 1963: A program for the assembly and display of radar-echo distributions. J. Appl. Meteorol., 2, 5, October, 582-593.
- Kuo, H. L., 1965: On formation and intensification of tropical cyclones through latent heat release by cumulus convection. J. Atmos. Sci., 22, 1, 40-63.
- Leese, John A., and Edward Epstein, 1963: Application of two-dimensional spectral analysis to the quantification of satellite cloud photographs. J. Appl. Meteorol., 2, 5, October, 629-644.
- Miller, B. I., 1969: Experiment in forecasting hurricane development with real data. Nat'l. Hurr. Res. Proj., Rept. No. 85.

APPENDIX A

A METHOD OF FOLLOWING PATTERN CLOUDS ON SEQUENTIAL SATELLITE PHOTOGRAPHS

John C. Freeman and Troxel Ballou

A. Discussion

The recent spectacular success of the ATS-1 and ATS-3 synchronous satellites has made it obvious that clouds can be photographed over large areas. This appendix outlines one numerical method for determining motions of clouds from these photographs.

The current most accepted method of following cloud motions for the purpose of making research studies is to make a movie from the ATS photographs and follow the cloud motion in the movie. The most useful of these movies have been made by Fujita. Similar devices involving flickers of these photographs have been developed in the National Environmental Satellite Center.

The problem of determining the motion of clouds is part of the satellite photograph modeling problem. The method described here has not been investigated sufficiently to give any idea of its feasibility or its expense but it seems worthy of including in this appendix as a guide to future discussion. The method requires the following equipment:

- a. A light intensity integrator with digital output
- b. An electronic computer

c. Image reproducing equipment

If a forecast system is being developed the measured cloud speeds would be used to move the cloud patterns. This could be done in a selective way by printing the matrices for the speed maxima. An example of how this works is shown.

This method of pattern following and especially recognition of patterns has been advanced in closely related forms by Kessler and Russo (1963), Leese and Epstein (1963) and Armijo (1966). However the method described here is simpler and has a more topical objective than any of those.

B. Procedure for Analysis of Cloud Movement on Satellite Radar

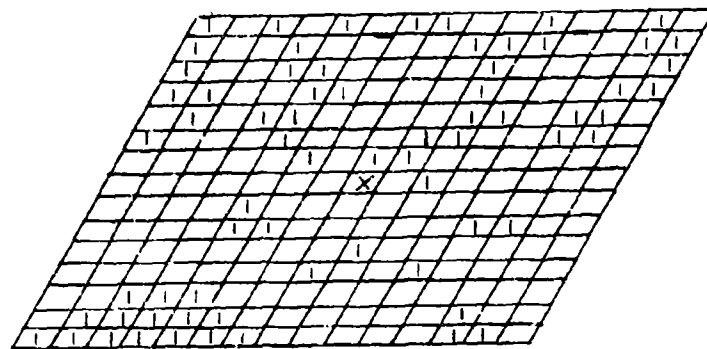
Cloud Maps

1. Select two maps of the same area at times t_1 and t_2 .
2. Select a large grid mesh (e.g. 10-20 degrees).
3. Divide it into gridpoints no more than 1/10 the size of the large grid.
4. Digitize the data at each gridpoint of both maps into binary digits by some criterion (such as "clouds/no clouds" present at that gridpoint).
5. Select a small grid mesh for correlating (see 6). A reasonable size would be five times the gridpoint spacing; an odd number greater than three is recommended.

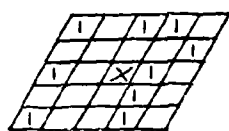
6. For each gridpoint away from the boundary (for points near the boundary, the overlay extends past the boundary) correlate the data at surrounding points in this manner:
 let k range from $i - 1$ to $i + 1$
 let ℓ range from $j - 1$ to $j + 1$
 for all combinations of $t_{2_{k\ell}}$ overlaid by $t_{1_{ij}}$,
 define the number $s_{k\ell}$ as the sum of the product $t_{1_{mn}} t_{2_{mn}}$ for all m, n under the sample grid.
7. Of these nine sums, the largest gives the magnitude of a vector with direction numbers $(k - i, \ell - j)$ which indicates the trend of cloud motion at $t_{1_{ij}}$.

Example:

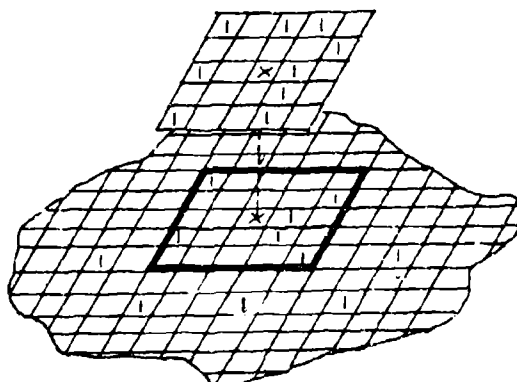
Figure 30a shows a 15^0 square grid with gridpoints 1^0 apart. Blank squares contain zeroes, other squares, ones, x indicates the center. Select a sampling grid 5^0 square (Figure 30b). At the point (i, j) overlay $t_{1_{ij}}$ onto $t_{2_{k\ell}}$ (Figure 30c). For the 25 squares that overlap, take the product of each top square with the one directly below it (Figure 31). Sum these 25 numbers and call the sum $s_{k\ell}$. In this example, $s_{k\ell}$ is 4. Repeat this procedure eight more times, superimposing $t_{1_{ij}}$ on each of the eight points surrounding $t_{2_{k\ell}}$. Note that to do this it is necessary to have values for an extra gridpoint all the way around the section of t_2 grid which is overlaid.



(a)



(b)



(c)

Figure 30 Binary digitized map of satellite radar cloud photographs. (a) Full grid, with binary digitized data. (b) Sampling grid from t_1 centered at t_{1ij} . (c) Grid around $t_{2k\ell}$ overlaid by sampling square centered at t_{1ij} .

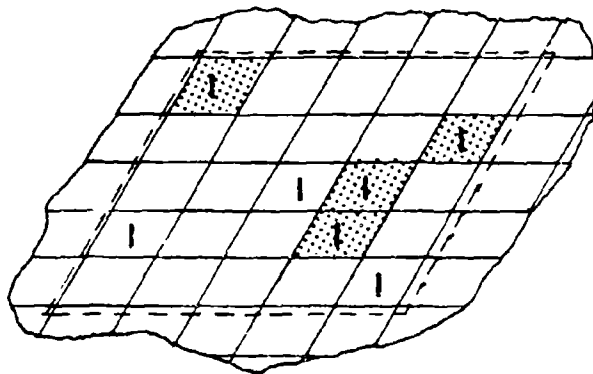
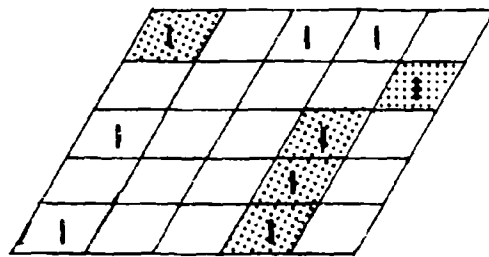


Figure 31 Section from Figure 30(c). Since there are four positions containing ones at coincident gridpoints above and below, the sum s_{k2} is 4.

Define a vector which points from $t_{i,j}$ to the maximum or center of gravity of these nine sums, and has a magnitude equal to that maximum: e.g., if the maximum sum was at $t_{i+1,j-1}$, the direction numbers of the vector would be $(1,-1)$, and its magnitude $s_{i+1,j-1}$. This vector is the primary gross-scale estimator of cloud movement.

Figures 32-34 show an actual example. The data were from two ESSA digitized mosaic maps for 29 and 30 May, 1969 at 2000Z (Figures 35 and 36). The original grid was 10° square, the gridpoint spacing 1° , and the sampling grid size 4° (5 would have been too large for this small a grid; 4 was small enough, but difficult to manipulate). Figure 32 shows the grid after all the sums have been taken. The nine numbers in each square (blanks indicate zeroes) are the magnitude of the vector pointing in that direction from the center of the square. For instance, in the square at $75^\circ\text{W } 24^\circ\text{N}$, the 5 means that when $t_{175,24}$ was overlaid onto $t_{275,25}$, there were 5 squares that matched (with ones). With $t_{175,24}$ overlaid on $t_{274,25}$, there were 4 matches.

In Figure 33, the highest number and the primary trend has been removed to show secondary trends.

In Figure 34, the highest number and the secondary trend in Figure 33 has been removed to show tertiary trends.

The variance in the direction of the vectors is explained by the fact that each is weighted according to the distance and magnitude of the numbers in that square.











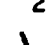














		W Longitude				
		77°	76°	75°	74°	73°
N Latitude	27°					
	26°					
	25°					
	24°					
	23°					

Figure 32 Example of procedure with actual data inserted.

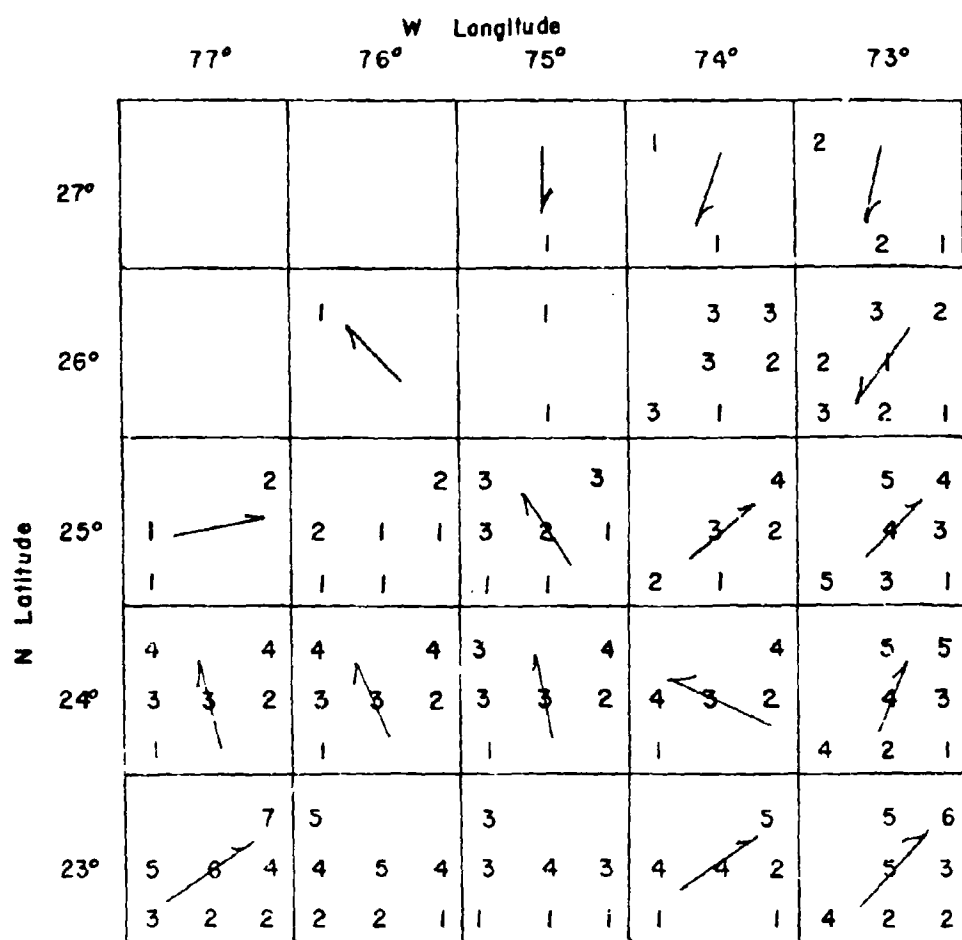


Figure 33 Figure 32 with highest numbers removed to indicate secondary trends.

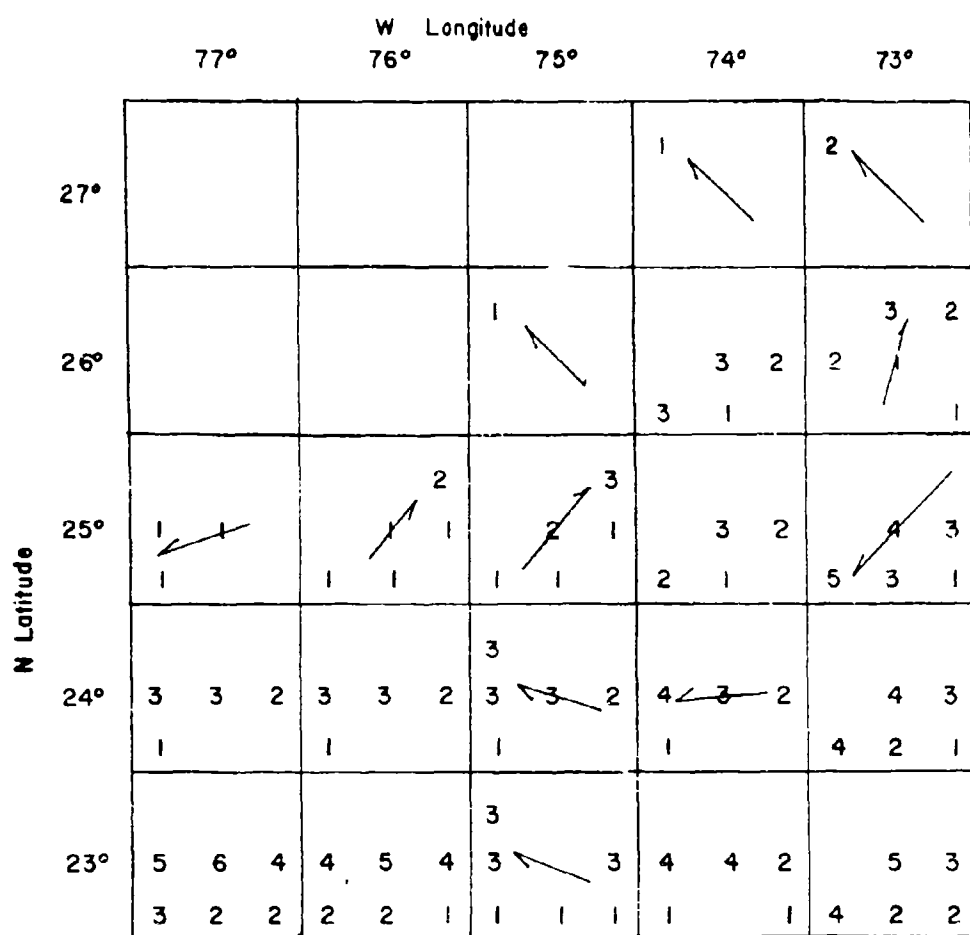


Figure 34 Figure 33 with highest remaining numbers removed to indicate tertiary trends.

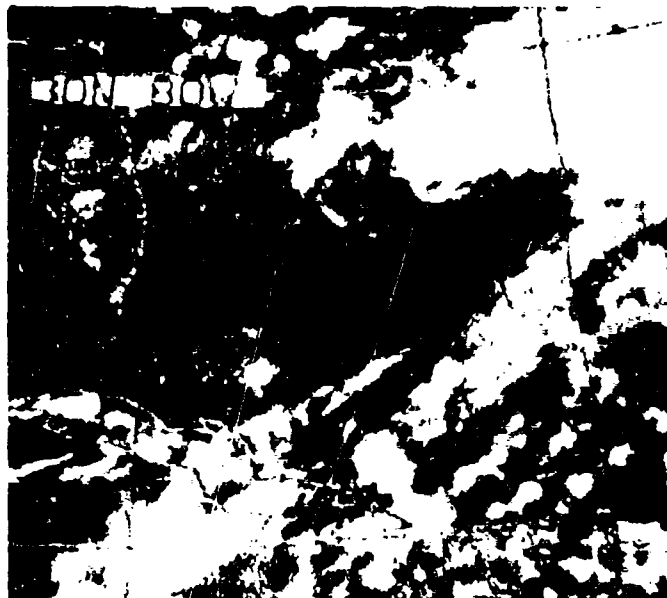


Figure 35 ESSA digitized mosaic map from 2000Z 29 May 1969.

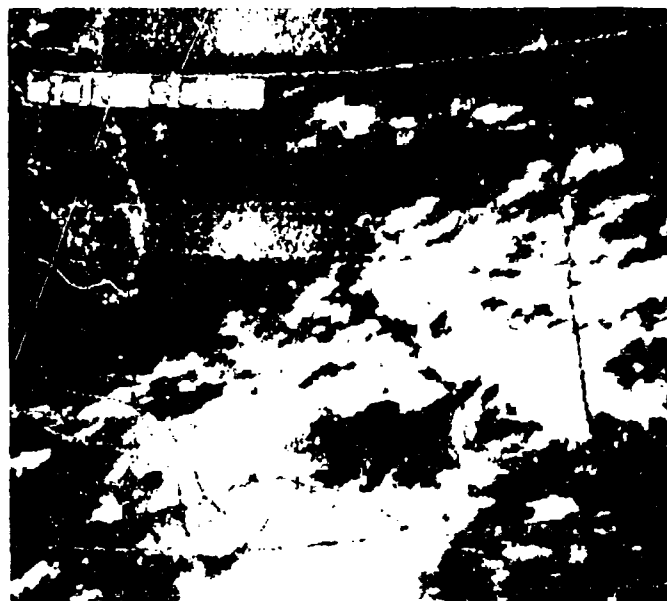


Figure 36 ESSA digitized mosaic map from 2000Z 30 May 1969.

APPENDIX B

SATELLITE OBSERVED CLOUDS AS STREAK LINES AND THE USE OF STREAK LINES AS A COORDINATE SYSTEM

John C. Freeman

ABSTRACT

The primary atmospheric model emphasized by the satellite is the streak line of high clouds that originate in equatorial regions and carries a jet stream of cloudy air all the way up into temperate latitudes. This streak line carries a companion dry streak* (to the north) that indicates that a systematic lineal disturbance of the atmosphere is closely related to these streak lines.

The carrying of very narrow zones over great distances and through latitude changes indicates that there is some scientific information to be gained by setting up a coordinate system based on the streak lines. Such a coordinate system could have the advantage of being visible on a satellite photograph and would make the following of physical phenomena by means of satellite data much easier than it is now.

The purpose of this appendix is to develop a workable system of following quantitative information in a streak line. The manuscript is available from the Institute for Storm Research.

*This has been discovered by NIMBUS infrared data, found and communicated to us by V. J. Oliver (personal communication, 1969).

Unclassified

Security Classification

DOCUMENT CONTROL DATA - R & D

(Security classification of title, body of abstract and indexing annotation must be entered when the overall report is classified)

1. ORIGINATING ACTIVITY (Corporate author)

Institute for Storm Research, Inc.
3812 Montrose Blvd.
Houston, Texas 77006

2a. REPORT SECURITY CLASSIFICATION

2b. GROUP

3. REPORT TITLE

FORECAST METHOD FROM SATELLITE PHOTOGRAPHS

4. DESCRIPTIVE NOTES (Type of report and inclusive dates)

Final Report - 1968-1969

5. AUTHOR(S) (First name, middle initial, last name)

John C. Freeman, Pieter Feteris, Sam Rosenberg, Keith Veigas, Troxel Ballou

6. REPORT DATE

June, 1969

7a. TOTAL NO. OF PAGES

59

7b. NO. OF REFS

8

8a. CONTRACT OR GRANT NO.

N 62306-68-C-0289

b. PROJECT NO.

9 999-8102-2080

c.

d.

9a. ORIGINATOR'S REPORT NUMBER(S)

ISR-45

9b. OTHER REPORT NO(S) (Any other numbers that may be assigned this report)

10. DISTRIBUTION STATEMENT

Distribution of this document is unlimited.

11. SUPPLEMENTARY NOTES

12. SPONSORING MILITARY ACTIVITY

Naval Air Systems Command
Project FAMOS, U.S. Fleet Weather Center
Navy Dept., Washington, D.C. 20390

13. ABSTRACT

Two models of atmospheric flow, "compensation" and "moist over-compensation" are found to be useful in the study of tropical weather in conventional and satellite observations. A numerical weather prediction model simulating important physical processes in the low latitudes is developed to test the feasibility of using ATS information to infer future weather distribution. Diagnostic studies using ATS films and conventional synoptic weather maps describe the weather situations in the Central North Pacific in terms of the theoretical models. Results of the prediction experiment and future use of ATS type data in numerical prediction models are discussed and application recommended. Appendix A gives a description of one method of following cloud motion in satellite photographs.